

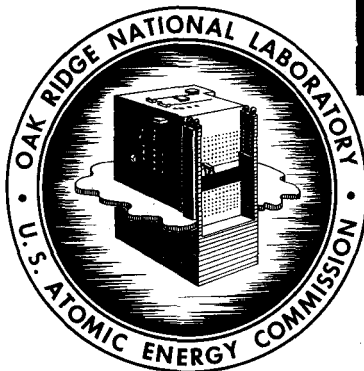
3 4456 0050330 0

12/T
CENTRAL RESEARCH LIBRARY
DOCUMENT COLLECTION

ORNL-3714, Vol. II
UC-34 - Physics
TID-4500 (35th ed.)

NEUTRON PHYSICS DIVISION
ANNUAL PROGRESS REPORT
FOR PERIOD ENDING AUGUST 1, 1964

CENTRAL RESEARCH LIBRARY
DOCUMENT COLLECTION
LIBRARY LOAN COPY
DO NOT TRANSFER TO ANOTHER PERSON
If you wish someone else to see this
document, send in name with document
and the library will arrange a loan.



OAK RIDGE NATIONAL LABORATORY
operated by
UNION CARBIDE CORPORATION
for the
U. S. ATOMIC ENERGY COMMISSION

Printed in USA. Price \$3.00. Available from the Clearinghouse for Federal
Scientific and Technical Information, National Bureau of Standards,
U.S. Department of Commerce, Springfield, Virginia

LEGAL NOTICE

This report was prepared as an account of Government sponsored work. Neither the United States, nor the Commission, nor any person acting on behalf of the Commission:

- A. Makes any warranty or representation, expressed or implied, with respect to the accuracy, completeness, or usefulness of the information contained in this report, or that the use of any information, apparatus, method, or process disclosed in this report may not infringe privately owned rights; or
- B. Assumes any liabilities with respect to the use of, or for damages resulting from the use of any information, apparatus, method, or process disclosed in this report.

As used in the above, "person acting on behalf of the Commission" includes any employee or contractor of the Commission, or employee of such contractor, to the extent that such employee or contractor of the Commission, or employee of such contractor prepares, disseminates, or provides access to, any information pursuant to his employment or contract with the Commission, or his employment with such contractor.

ORNL-3714, Vol.II

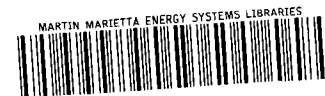
Contract No. W-7405-eng-26

**NEUTRON PHYSICS DIVISION
ANNUAL PROGRESS REPORT
For Period Ending August 1, 1964**

E. P. Blizard, Director
A. D. Callihan, Associate Director
F. C. Maienschein, Associate Director

DECEMBER 1964

OAK RIDGE NATIONAL LABORATORY
Oak Ridge, Tennessee
operated by
UNION CARBIDE CORPORATION
for the
U. S. ATOMIC ENERGY COMMISSION



3 4456 0050330 0



Preface

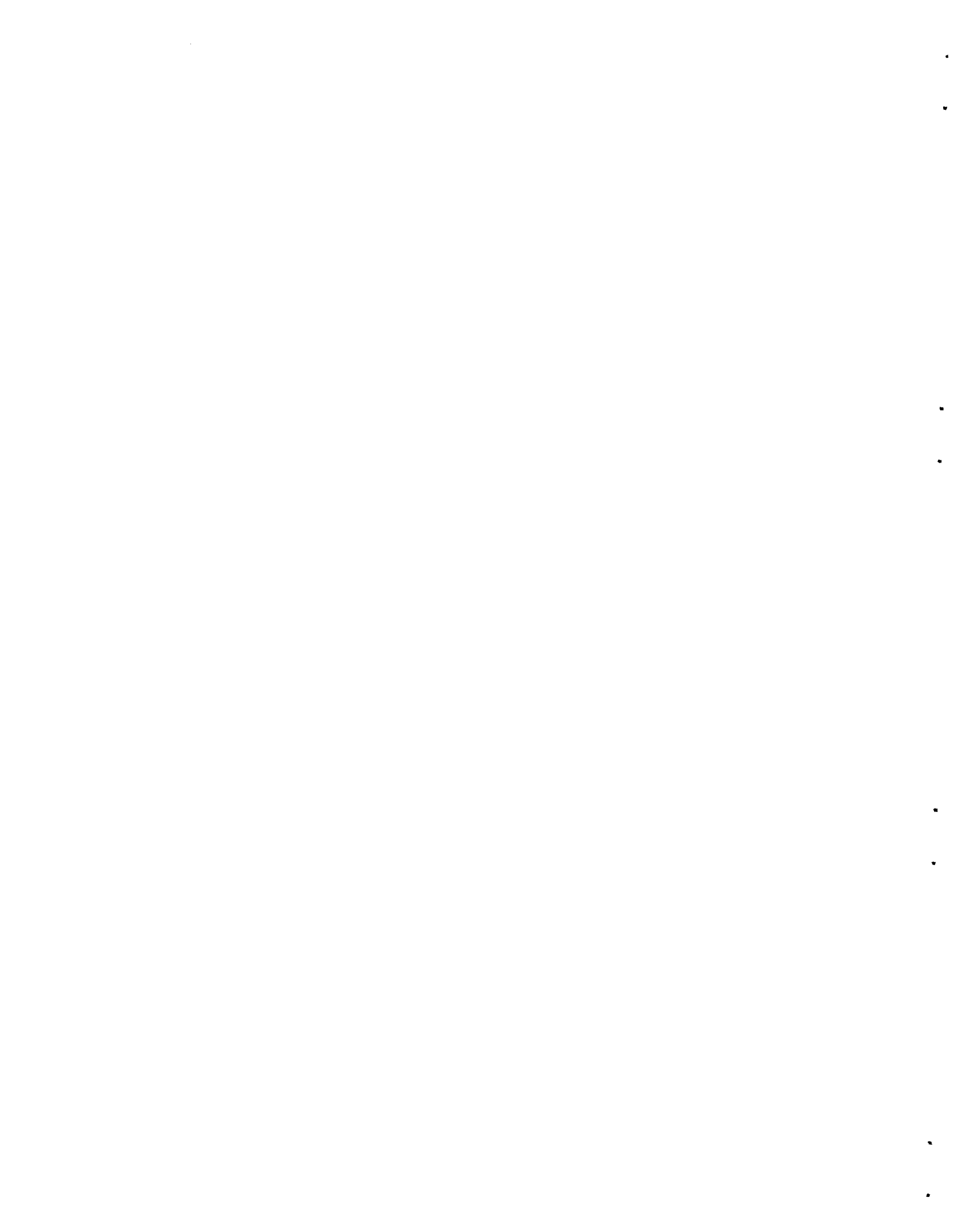
For the second consecutive year the Neutron Physics Division is issuing its annual progress report in two volumes, with the papers describing research performed in the high-energy radiation shielding program collected in Volume II. Again this separation is made primarily to aid our readers, most of whom we believe to be interested in the work reported in one volume only. It is not prompted by the size of the report, for, as you have already realized, the number of pages in this year's report has decreased considerably below that in our previous reports. This decrease reflects a change in the Division's procedure for reporting research performed during the year. It has become increasingly apparent that emphasis on the annual progress report has resulted in some of our research not being reported elsewhere, an effect which we deplore. The lack of other publications is made even less desirable by the fact that the individual papers of progress reports are not treated specifically by information centers or otherwise collated into the organized scientific literature. Therefore, in planning our report this year, we decided to limit each paper to the length of either an abstract or a summary in order to give the authors more time to spend on "topical" reports. In fact, we had hoped that for each abstract included in the annual report a separate detailed report or journal article would have already been published, but unfortunately the attractiveness of not duplicating writing efforts resulted in so great an influx of topical reports to our publications staff that it became impossible to handle all of them prior to the publication of the

annual report. It can be presumed, however, that for each abstract included in the annual report the publication of a topical report is imminent. Those papers which are not identified as abstracts are summaries that describe work which is still in progress and thus is not yet ready for publication in a topical report.

In a few cases, the reader will notice that abstracts are included which report work that was described in last year's annual report. We have allowed this duplication intentionally so that we might call your attention to the fact that topical reports on these particular subjects have now been issued. This is a practice we will not repeat next year, however, since we assume that the abstract in this year's report will be sufficient notice of the forthcoming document.

NOTE

The work described in this volume was performed either to aid in the design of shields for high-energy accelerators or to investigate the interactions of high-energy radiations in materials proposed for space vehicle shields. In some cases both purposes are served. The accelerator shielding work is supported by the Research Division of the Atomic Energy Commission, and the space radiation shielding studies are supported by the National Aeronautics and Space Administration under NASA Order R-104.



Contents

8.	THEORETICAL STUDIES OF HIGH-ENERGY RADIATION SHIELDING	97
8.1.	The Nucleon Transport Code, NTC – W. E. Kinney	97
8.2.	Calculated Tissue Current-to-Dose Conversion Factors for Nucleons of Energy Below 400 Mev – W. E. Kinney and C. D. Zerby.....	97
8.3.	A Note on Importance Functions for the Shielding of Manned Space Vehicles – R. G. Alsmiller, Jr.....	99
8.4.	The Secondary Particle Contribution to the Dose from Monoenergetic Proton Beams and the Validity of Current-to-Dose Conversion Factors – D. C. Irving, R. G. Alsmiller, Jr., W. E. Kinney, and H. S. Moran	99
8.5.	The Validity of the Straightahead Approximation in Space Vehicle Shielding Studies – R. G. Alsmiller, Jr., D. C. Irving, W. E. Kinney, and H. S. Moran.....	100
8.6.	Calculations for Estimating Neutron Doses from Low-Energy Solar Flare Protons – F. S. Alsmiller.....	104
8.7.	Error in Intranuclear Cascade Code for Incident Particle Energies from 25 to 350 Mev – H. W. Bertini	104
8.8.	Intranuclear Cascade Calculations for Incident Particle Energies from 25 Mev to 2 Gev – H. W. Bertini	105
8.9.	Rapid Computation of Specific Energy Losses for Energetic Charged Particles – R. W. Peelle	110
8.10.	Energy Deposited by High-Energy Electrons in an LiF Optical System of the Orbiting Astronomical Observatory – H. S. Moran, C. D. Zerby, and F. C. Maienschein	110
8.11.	Calculation of the Flux of Neutrons Diffusing Beneath the Shield ("Earthshine") of a Meson Factory – W. E. Kinney	111
8.12.	A Solution to the Nucleon-Meson Cascade Equations Under Very Special Conditions – R. G. Alsmiller, Jr.	112
8.13.	Numerical Solutions of the One-Dimensional Nucleon-Meson Cascade Equations – R. G. Alsmiller, Jr., J. E. Murphy, and J. Barish	113
8.14.	Nucleon-Meson Cascade Calculations: Transverse Shielding for a 45-GeV Electron Accelerator (Part IV) – R. G. Alsmiller, Jr., F. S. Alsmiller, and J. Barish	115
8.15.	Analytic Solutions to Nucleon-Meson Cascade Equations for Special Cases of Secondary Particle Production Kernels – F. S. Alsmiller	115
8.16.	Statistical Model Calculations of Nucleon-Nucleon and Pion-Nucleon Collisions: Center-of-Mass Spectra – R. G. Alsmiller, Jr.	116
8.17.	Statistical Model Calculations of Nucleon-Nucleon and Pion-Nucleon Collisions: Laboratory Energy-Angle Distributions Assuming Isotropy in the Center-of-Mass System – R. G. Alsmiller, Jr.....	116

8.18.	Nucleon-Nucleus and Pion-Nucleus Collisions in the Energy Range 2 to 10 Gev – R. G. Alsmiller, Jr.	116
8.19.	Pair Production Cross-Section Program – C. D. Zerby and C. W. Nestor, Jr.	117
8.20.	Statistical Fluctuations in the Output of an Intranuclear Cascade Monte Carlo Computation – R. W. Peelle	117
8.21.	Differential Bremsstrahlung Cross Sections for Low-Energy Electrons – J. D. Lawson	118
8.22.	Space Vehicle Shielding Studies (Part III): The Attenuation of a Particular Solar Flare by an Aluminum Shield – R. G. Alsmiller, Jr., and J. E. Murphy	118
9.	EXPERIMENTAL STUDIES FOR HIGH-ENERGY RADIATION SHIELDING	119
9.1.	The Space, Time, and Energy Distributions of the Proton Beam of the Harvard University Synchrocyclotron – R. T. Santoro	119
9.2.	Measurement of the Intensity of the Proton Beam of the Harvard University Synchrocyclotron for Energy-Spectral Measurements of Nuclear Secondaries – R. T. Santoro and R. W. Peelle	119
9.3.	Spectra of Gamma Rays Produced by the Interaction of ~160-Mev Protons with Be, C, O, Al, Co, and Bi – W. Zobel, F. C. Maienschein, and R. J. Scroggs	120
9.4.	Differential Cross Sections by Flight-Time Spectroscopy for Proton Production in Reactions of 160-Mev Protons with Various Nuclei – R. W. Peelle, T. A. Love, N. W. Hill, and R. T. Santoro	120
9.5.	Spectra of Neutrons and Protons from Targets Bombarded by 160-Mev Protons – J. W. Wachter, W. A. Gibson, W. R. Burrus, and C. F. Johnson.....	122
9.6.	Comparison of Measured Neutron and Proton Spectra with Calculated Spectra in the Energy Region Between 50 and 160 Mev – W. A. Gibson, W. R. Burrus, W. E. Kinney, J. W. Wachter, and C. F. Johnson	124
9.7.	Spectra of Neutrons and Protons from Targets Bombarded by 450-Mev Protons – W. A. Gibson, W. R. Burrus, and J. W. Wachter	126
9.8.	Measurements of Proton-Induced Gamma-Ray Spectra at ORIC – W. Zobel, J. H. Todd, R. T. Santoro, and F. C. Maienschein.....	128
9.9.	The Energy Deposition in a Water-Filled Spherical Phantom by Secondaries from High-Energy Protons and by Neutrons – T. V. Blosser, F. C. Maienschein, and R. M. Freestone, Jr.	130
9.10.	Results from Nuclear Emulsions Embedded in a Steel Shield Exposed to a 10-GeV/c Proton Beam – R. L. Childers, C. D. Zerby, C. M. Fisher, and R. H. Thomas	130
9.11.	Differential and Total Cross Sections for the ${}^9\text{Be}(\alpha, n)$ Reactions from 6 to ~10 Mev – V. V. Verbinski, W. R. Burrus, J. K. Dickens, J. Gibbons, W. E. Kinney, R. L. Macklin, and F. G. Perey	131

10. RADIATION DETECTOR STUDIES (II).....	134
10.1. Measurement of the Absolute Efficiency of NE-213 Organic Phosphors for the Detection of 14.4- and 2.6-Mev Neutrons – T. A. Love, R. T. Santoro, R. W. Peelle, N. W. Hill, and R. J. Schuttler.....	134
10.2. Measurements of the Fast and Total Light Response of NE-213 Scintillators to Charged Particles – T. A. Love and R. J. Schuttler.....	136
10.3. Modification of a 400-Channel Pulse-Height Analyzer to Eliminate Storage of Pulses Having Energies Below a Preset Bias – H. A. Todd and T. A. Love.....	138
10.4. The Choice of Capacitors for Nanosecond Circuits – N. W. Hill and C. O. McNew.....	140
10.5. Progress in the Development of an Instrument-Response Unfolding Method – W. R. Burrus, B. D. Holcomb, and J. Replogle	140
10.6. A Sensitive Tunnel-Diode Discriminator – N. W. Hill	142
10.7. Strip-Line Construction for Nanosecond Circuitry – J. W. McConnell.....	142
10.8. Performance Characteristics of Modular Nanosecond Circuitry Employing Tunnel Diodes – N. W. Hill, R. J. Scroggs, J. W. McConnell, and J. M. Madison.....	143
10.9. Curled Light Pipes for Thin Organic Scintillators – W. A. Gibson	144
10.10. Nanosecond Light Sources for Gain Stabilization – J. W. McConnell	144
10.11. A Method for Making Inexpensive Thick Boron Targets to Obtain Gamma Rays from the $^{11}\text{B}(p,\gamma)^{12}\text{C}$ Reaction – R. T. Santoro and H. Weaver	145
10.12. Constant-Current Sources for Instrument Calibration – R. T. Santoro, F. E. Gillespie, R. J. Scroggs, and T. A. Love	145
10.13. Calculation of the Efficiency of Organic Scintillators for Fast Neutrons – R. J. Schuttler	145



8. Theoretical Studies of High-Energy Radiation Shielding

8.1. THE NUCLEON TRANSPORT CODE, NTC¹

W. E. Kinney

Detailed information concerning the interactions of high-energy nucleons with matter is of particular interest in the design of radiation shields for space vehicles and high-energy particle accelerators.

The Monte Carlo method has been applied to the calculation of such interactions in the construction of the Nucleon Transport Code (NTC), a linked series of newly written codes for treatment of high-energy transport and previously written codes for the treatment of neutrons of energies below 50 Mev. NTC, written for the IBM-7090 computer, calculates the transport of nucleons having initial energies as high as 400 Mev through complex arbitrary configurations containing a maximum of four media, each of which may be composed of up to ten isotopes. Cascade processes and particle evaporation from excited nuclei are taken into account. The end result of NTC is one or more magnetic tapes containing the detailed records of all quantities pertinent to the transport of the nucleon. These tapes can be independently analyzed by the individual user of NTC to produce desired solutions to specific problems.

Appendices include typical analysis routines; a list of tape assignments; a user's manual for the low-energy portion of the code and for the geometry routine; and a full-scale demonstration problem, complete in all details, which can be used to verify satisfactory performance by all parts of the code group.

References

¹Abstract of ORNL-3610 (August 1964).

8.2. CALCULATED TISSUE CURRENT-TO-DOSE CONVERSION FACTORS FOR NUCLEONS OF ENERGY BELOW 400 Mev

W. E. Kinney

C. D. Zerby¹

To evaluate the hazard to personnel who encounter radiation in space or near high-energy accelerators, it is necessary to know the distribution of energy deposition within the body resulting from the impinging radiations. Important regions of the depth-dose distribution are the surface dose for estimating skin and eye damage and the dose at a depth of 5 cm, which is the average depth of the blood-forming organs. In addition, the average whole-body dose is an important parameter of a depth-dose distribution to estimate overall damage.

A series of calculations has been performed to supply tissue current-to-dose conversion factors for incident neutrons and protons having energies in the range 60 to 400 Mev. A general set of factors was computed which may be applied to specific radiation fields to give upper and lower bounds to the surface and 5-cm-depth doses out to the average and maximum doses.

The model chosen for study was a 30-cm-thick slab of tissue infinite in its lateral dimensions. The calculations were performed by means of a series of Monte Carlo computer codes (Sect. 8.1). Nucleons were effectively introduced uniformly over one face of the slab both normally and isotropically to give doses which should bracket those resulting from actual angular distributions. The doses were computed by summing the energy deposited in unit cubes distributed through the slab in a direction normal to the surface. Ten

thousand source particles were run for each angular distribution and for each of the incident energies of 400, 300, 200, 100, and 60 Mev. Energy deposition was broken down into contributions from primary protons, secondary protons, and heavy nuclei. In order to permit freedom in choosing proton RBE as a function of energy, the proton rad dose was subdivided into contributions from protons having energies above 50 Mev, lying in the energy ranges 10 to 50 Mev, 5 to 10 Mev, and 1 to 5 Mev, and having energies below 1 Mev. The RBE's chosen in this study for these energy groups were 1, 1, 1.25, 3, and 8 respectively. Heavy nuclei were taken to have an RBE of 20.

The calculated doses were found to be in agreement with Shalnov's measurements² of dose in water and in paraffin due to nearly monoenergetic

140-Mev neutrons stripped from 280-Mev deuterons on copper and also due to neutrons resulting from the charge-exchange reaction of 480-Mev protons on beryllium (ref. 3).

The dose due to secondary particles increases with increasing primary beam energy since the secondary production increases. The average rem dose due to secondaries resulting from normally incident protons rises from 12.5% of the total dose at an incident energy of 100 Mev to 53% of the total dose at 400-Mev incident energy.

The data may be conveniently expressed by the following equations, where D is the dose, in rem, due to a current of one nucleon incident per square centimeter of surface, E is the energy, in Mev, and logarithms are taken to the base 10. The doses are as follows:

Log D for Various Cases

Normally Incident Protons

Average dose	$-7.72 + 6.4 \times 10^{-3}E - 1.1 \times 10^{-5}E^2$; $60 < E < 215$ $-6.20 - 4.3 \times 10^{-3}E + 5.5 \times 10^{-6}E^2$; $215 < E < 400$
5-cm depth dose	$-6.27 - 4.6 \times 10^{-3}E + 6.4 \times 10^{-6}E^2$; $80 < E < 400$
Surface dose	$-6.64 - 2.2 \times 10^{-3}E + 2.9 \times 10^{-6}E^2$; $60 < E < 400$
Maximum dose	$-6.02 - 1.2 \times 10^{-3}E$; $60 < E < 215$ $-6.62 - 1.1 \times 10^{-3}E$; $215 < E < 400$

Normally Incident Neutrons

Average dose	$-7.43 + 2.7 \times 10^{-4}E$; $60 < E < 400$
5-cm depth dose	-7.38 ; $60 < E < 400$
Surface dose	$-7.59 + 3.7 \times 10^{-4}E$; $60 < E < 400$
Maximum dose	$-7.35 + 3.8 \times 10^{-4}E$; $60 < E < 400$

Isotropically Incident Protons

Average dose	$-7.79 + 7.9 \times 10^{-3}E - 1.7 \times 10^{-5}E^2$; $60 < E < 215$ $-7.07 + 1.2 \times 10^{-3}E - 1.3 \times 10^{-6}E^2$; $215 < E < 400$
5-cm depth dose	$-6.57 - 5.4 \times 10^{-4}E$; $80 < E < 400$
Surface dose	$-6.30 - 2.7 \times 10^{-3}E + 3.7 \times 10^{-6}E^2$; $60 < E < 400$
Maximum dose	$-6.26 - 2.9 \times 10^{-3}E + 4.1 \times 10^{-6}E^2$; $60 < E < 400$

Isotropically Incident Neutrons

Average dose	$-7.26 + 5.6 \times 10^{-4}E$; $60 < E < 400$
5-cm depth dose	$-7.18 + 3.9 \times 10^{-4}E$; $60 < E < 400$
Surface dose	$-7.26 + 4.5 \times 10^{-4}E$; $60 < E < 400$
Maximum dose	$-7.18 + 4.0 \times 10^{-4}E$; $60 < E < 400$

References

¹Union Carbide Research Institute, Tarrytown, N.Y.

²M. I. Shalnov, *Soviet J. At. Energy (English Transl.)* **5**, 735 (June 1958).

³V. P. Dzhelepov *et al.*, *Izv. Akad. Nauk SSSR Ser. Fiz.* **19**, 573 (1955).

8.3. A NOTE ON IMPORTANCE FUNCTIONS FOR THE SHIELDING OF MANNED SPACE VEHICLES¹

R. G. Alsmiller, Jr.

Results were given in another report² for two importance functions of interest in the shielding of manned space vehicles. This report¹ discusses the various importance functions which may be defined and gives calculations for several of these functions. While the functions discussed in the previous report were concerned with the dose from primary and secondary particles which emerge from the surface of an aluminum shield, the functions given in this report are concerned with the dose from primary and secondary particles in tissue that arise from a primary proton beam that has penetrated an aluminum shield. The calculations are based on the tissue dose calculations of Kinney and Zerby (Sect. 8.2). The results refer specifically to primary proton beams which are normally incident on slab shields and yield little if any information about the more general case of isotropic incidence.

References

¹Abstract of ORNL-3583 (March 1964).

²R. G. Alsmiller, Jr., and J. E. Murphy, *Space Vehicle Shielding Studies: Calculations of the Attenuation of a Model Solar Flare and Monoenergetic Proton Beams by Aluminum Shields*, ORNL-3317 (1963).

8.4. THE SECONDARY PARTICLE CONTRIBUTION TO THE DOSE FROM MONOENERGETIC PROTON BEAMS AND THE VALIDITY OF CURRENT-TO-DOSE CONVERSION FACTORS

D. C. Irving

R. G. Alsmiller, Jr.

W. E. Kinney

H. S. Moran

In shielding studies for manned space vehicles the presence of secondary particles introduces considerable complexity into the calculations. It is very desirable therefore to determine the magnitude of the contribution of these secondary particles in special cases in order to determine whether or not they may reasonably be neglected. It is also desirable to distinguish between the secondary particles produced in the shield and those produced in the astronaut, since the latter may, at least approximately, be taken into account by the appropriate use of current-to-dose conversion factors.

In the energy region 100 to 400 Mev, calculations have been carried out for monoenergetic proton beams incident isotropically on a slab shield followed by a 30-cm-thick slab of tissue. The primary proton, secondary proton, and neutron fluxes (gamma rays are not considered) at the shield-tissue interface have been calculated, and the dose (both in rads and rems) has been determined as a function of depth in the tissue from each of these three beams. Furthermore, the dose as a function of depth in the tissue from each of these three fluxes has been decomposed into a "primary" contribution in the tissue (that is, a contribution from atomic ionization and excitation) and a secondary contribution (a contribution from elastic and non-elastic nuclear collisions).

The doses discussed above were obtained by direct computation; that is, the particles were transported through the tissue and their energy deposition was recorded as a function of depth. An alternate procedure is to obtain the doses by applying current-to-dose conversion factors to the currents which emerge from the shield. Such conversion factors are available only for proton and neutron beams which are incident either normally or isotropically on the tissue. The beams leaving

Table 8.4.1. Calculated Doses for 400-Mev Protons Isotropically Incident on a 30-g/cm²-thick Slab of Aluminum Followed by Tissue

	Actual Dose	Dose Calculated	
		With Normal Incidence Conversion Factor	With Isotropic Incidence Conversion Factor
Average Dose (rads)			
Primary protons	0.300×10^{-7}	0.235×10^{-7}	0.326×10^{-7}
Secondary protons	0.444×10^{-8}	0.416×10^{-8}	0.447×10^{-8}
Secondary neutrons	0.164×10^{-8}	0.126×10^{-8}	0.185×10^{-8}
Total	0.361×10^{-7}	0.289×10^{-7}	0.389×10^{-7}
Average Dose (rems)			
Primary protons	0.452×10^{-7}	0.316×10^{-7}	0.446×10^{-7}
Secondary protons	0.614×10^{-8}	0.543×10^{-8}	0.594×10^{-8}
Secondary neutrons	0.793×10^{-8}	0.616×10^{-8}	0.832×10^{-8}
Total	0.592×10^{-7}	0.432×10^{-7}	0.588×10^{-7}
5-cm-deep Dose (rads)			
Primary protons	0.338×10^{-7}	0.214×10^{-7}	0.409×10^{-7}
Secondary protons	0.745×10^{-8}	0.562×10^{-8}	0.791×10^{-8}
Secondary neutrons	0.201×10^{-8}	0.140×10^{-8}	0.230×10^{-8}
Total	0.433×10^{-7}	0.284×10^{-7}	0.512×10^{-7}
5-cm-deep Dose (rems)			
Primary protons	0.517×10^{-7}	0.314×10^{-7}	0.557×10^{-7}
Secondary protons	0.104×10^{-7}	0.732×10^{-8}	0.104×10^{-7}
Secondary neutrons	0.109×10^{-7}	0.746×10^{-8}	0.108×10^{-7}
Total	0.730×10^{-7}	0.462×10^{-7}	0.768×10^{-7}

the shield and entering the tissue do not necessarily have either of these angular distributions, and therefore the doses obtained by using these conversion factors must be considered to be approximate. The doses at a depth of 5 cm and the average whole-body doses have been calculated, with the proton beams assumed to be both normally and isotropically incident on the tissue.

Typical results obtained by using the conversion factors are compared with direct-computation results in Table 8.4.1 for the case of a 400-Mev proton beam isotropically incident on a 30-g/cm² thick slab of aluminum followed by tissue.

8.5. THE VALIDITY OF THE STRAIGHTHEAD APPROXIMATION IN SPACE VEHICLE SHIELDING STUDIES

R. G. Alsmiller, Jr.
D. C. Irving

W. E. Kinney
H. S. Moran

Many of the shielding studies for manned space vehicles have been carried out in what is usually called the straighthead approximation.¹ This approximation greatly simplifies the computation, but its use necessarily introduces inaccuracies. To test the validity of the approximation, calculations

have been carried out and compared with results obtained with the angular distribution of the secondary particles properly taken into account.

To define the approximation as it is used here, we note that, in general,

$$F_{ij} = F_{ij}(E', E, \Omega' \cdot \Omega), \quad (1)$$

where F_{ij} is the number of particles of type i per unit energy range per unit solid angle possessing kinetic energy E and direction given by the unit vector Ω after a particle of type j with kinetic energy E and direction Ω' undergoes either an elastic or a nonelastic collision.

In the straightahead approximation the quantity F_{ij} is approximated by

$$F_{ij}(E', E, \Omega' \cdot \Omega) = f_{ij}(E', E) \frac{\delta(\Omega' \cdot \Omega - 1)}{2\pi}, \quad (2)$$

where

$$f_{ij}(E', E) = \int_0^\pi \int_0^{2\pi} F_{ij}(E', E, \Omega' \cdot \Omega) d\Omega. \quad (3)$$

The delta function in Eq. (2) ensures that all emergent particles have the same direction as the incident particle, and Eq. (3) follows from integrating Eq. (2) over all solid angles. It must be carefully noted that as defined here the straight-ahead approximation applies to both elastic and nonelastic collisions. Furthermore, *all* emergent

UNCLASSIFIED
ORNL DWG. 64-9309

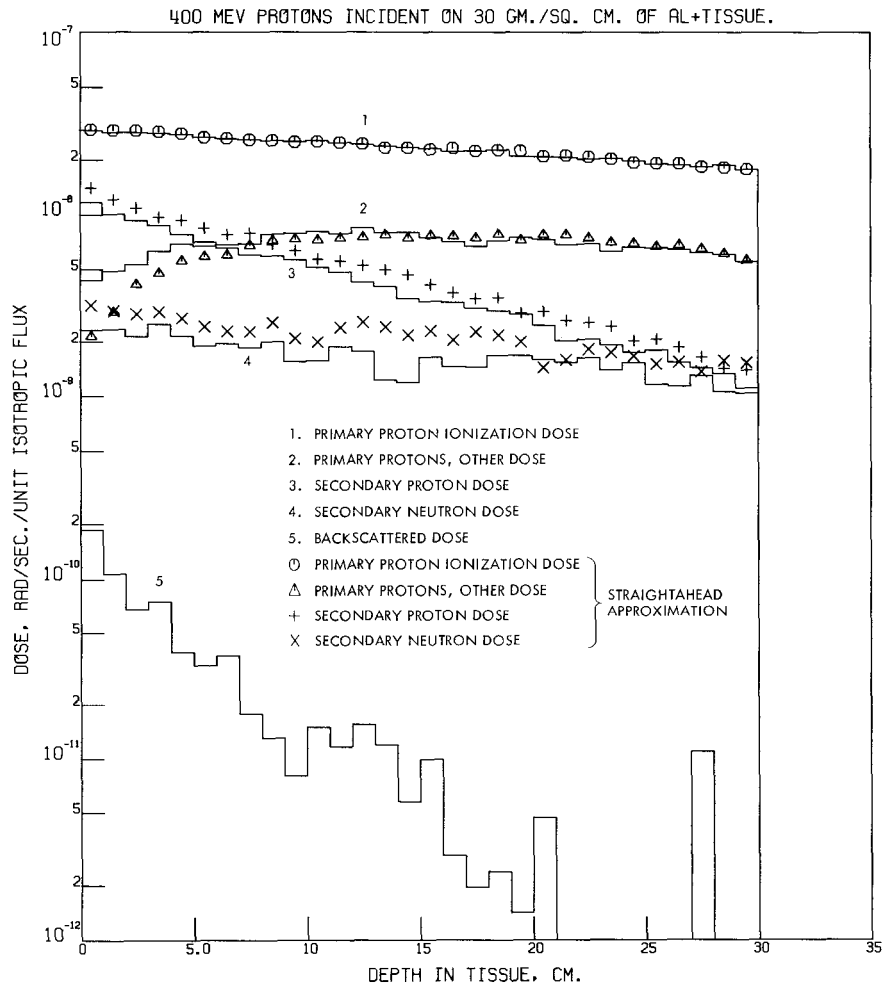


Fig. 8.5.1. Comparison of Straightahead Dose Results with Exact Results (in Rads) for the Case of 400-Mev Protons Isotropically Incident on a 30-g/cm²-thick Slab of Aluminum Followed by a Slab of Tissue.

particles are assumed to go in the forward direction; that is, no attempt is made to discriminate against those particles which are emitted in the backward quadrant.

To ensure that any difference which exists between the approximate and the exact calculation is due to the approximation being considered and not to differences in nuclear data, the straight-ahead calculations presented here have been carried out with the NTC code (Sect. 8.1) with which the exact calculations were done. The only change made in the code was in the angular distribution of the scattered particles.

In Fig. 8.5.1 the results of the approximate and exact calculations are compared for the case of a 400-Mev proton beam isotropically incident on a

30-g/cm²-thick slab of aluminum followed by a 30-cm slab of tissue. The solid curves are the results of the exact calculations, while the plotted points are the results of the approximate calculations. The primary proton, secondary proton, and secondary neutron fluxes incident on the tissue are defined to be those fluxes which would emerge from the aluminum if the tissue were absent. The dose as a function of depth in the tissue is broken into five contributions:

1. the primary proton ionization dose,
2. the dose from secondary particles produced by primary protons in the tissue,
3. the secondary proton dose,

UNCLASSIFIED
ORNL DWG. 64-9311

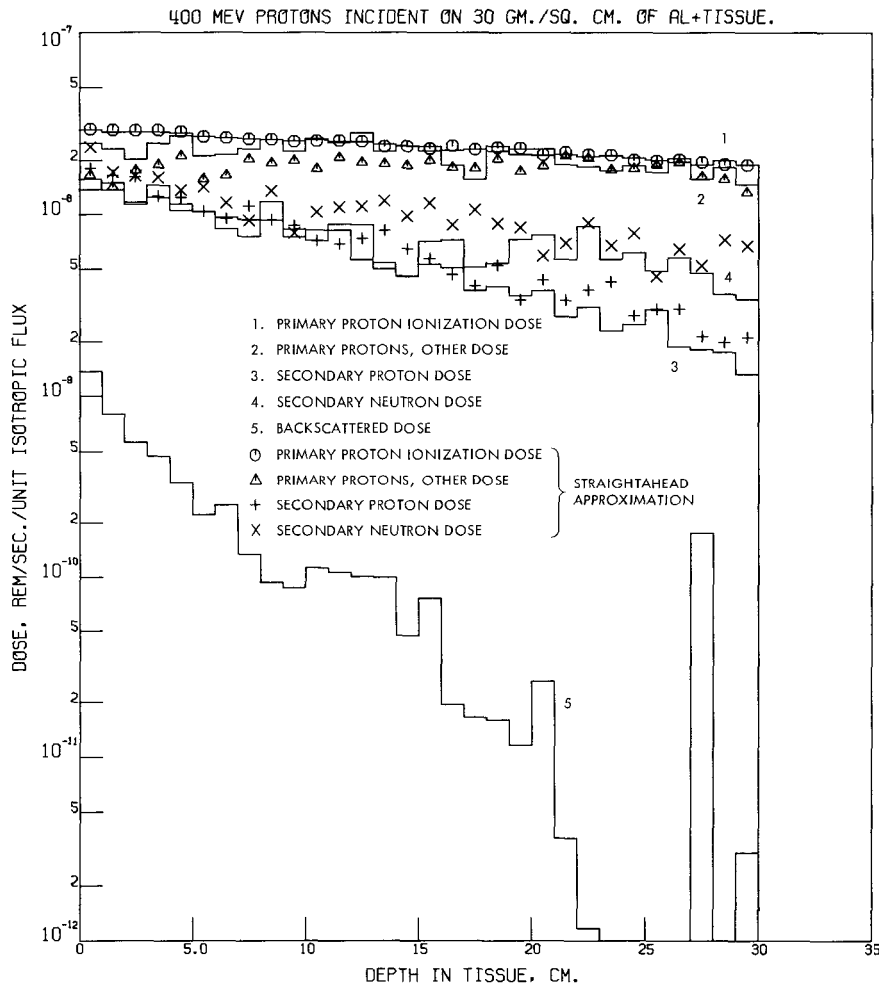


Fig. 8.5.2. Comparison of Straighthead Dose Results with Exact Results (in Rems) for the Case of 400-Mev Protons Isotropically Incident on a 30-g/cm²-thick Slab of Aluminum Followed by a Slab of Tissue.

4. the secondary neutron dose,
5. the backscattered dose, that is, the dose from all particles which are produced in the tissue and cross into the aluminum.

Since the primary protons travel in a straight line (multiple Coulomb scattering was not included in the calculation), the exact and approximate calculations give the same results for the primary proton ionization dose. The secondary proton and secondary neutron doses from the approximate calculations are slightly larger than those from the exact calculations, particularly in the first few centimeters of tissue, while the dose from secondary particles produced by primary protons is smaller than the dose in the exact calculations in

the first few centimeters. There is, of course, no approximate backscattered dose.

In Fig. 8.5.2 the calculations are compared for the same case as in Fig. 8.5.1, but the dose is given in rems rather than rads. The rem calculation is carried out in the same manner as that described by Kinney and Zerby (Sect. 8.2). The agreement between the exact and approximate calculations is roughly the same as in Fig. 8.5.1.

The results for 100-Mev protons isotropically incident on a 10-g/cm²-thick slab of aluminum followed by a 30-cm-thick slab of tissue are given in Fig. 8.5.3. In this case the primary protons do not penetrate the shield; so we have exact doses only from secondary protons, secondary neutrons,

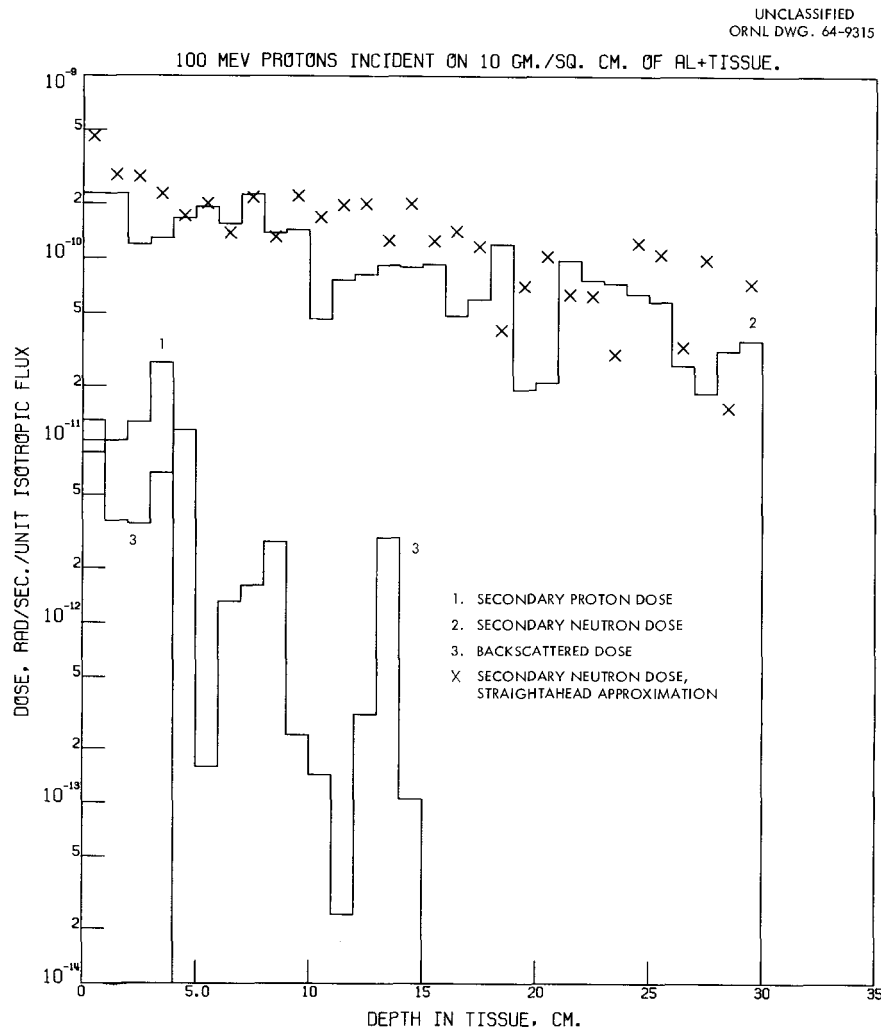


Fig. 8.5.3. Comparison of Straighthead Dose Results with Exact Results for the Case of 100-Mev Protons Isotropically Incident on a 10-g/cm²-thick Slab of Aluminum Followed by Tissue.

and backscattered particles. In fact, the approximate secondary proton dose is zero within the statistics; so only the secondary neutron doses can actually be compared. The approximate secondary neutron dose is somewhat too large in this case, as it was in Fig. 8.5.1.

In the cases presented here the straighthead approximation appears to be quite good. The approximation usually overestimates the dose and appears to have essentially the same validity for elements between carbon and copper. However, it would be inadvisable to draw very general conclusions based on so few computations. It must be remembered that the low-energy region (<100 Mev) is still to be treated and may be important in the study of typical flare spectra.

References

¹For an extensive list of references see: S. P. Shen, *Astronaut Acta* **9**, 28 (1963).

8.6. CALCULATIONS FOR ESTIMATING NEUTRON DOSES FROM LOW-ENERGY SOLAR FLARE PROTONS

F. S. Alsmiller

The low-energy portion of the solar flare proton spectrum (<40 Mev) is not generally considered a hazard in space shielding problems because it is readily stopped by thin shields (<2 g/cm² of Al). Also, since at these energies the proton ranges are much shorter than the collision mean free paths, the probability for secondary particle production is less than it would be for the higher energy protons in all but the thinnest portions of the shield. Even so, the fact that the total number of solar protons below 40 or 50 Mev may be factors of 10 greater than the number above these energies means that at least the first generation of neutrons they produce may contribute appreciably to the dose, since neutrons have a good chance of penetrating the shield.

Experimental information regarding the total neutron yield and spectrum from low-energy proton reactions in light elements is generally lacking. Two theoretical models, whose results are being

compared, are available at ORNL as Monte Carlo computer codes. The first utilizes a code prepared by Dresner¹ to predict the evaporation neutron spectrum from the compound nucleus formed by the incident proton and the target nucleus, with excitation energy taken to be the proton kinetic energy plus its binding energy in the compound nucleus. The second is an intranuclear cascade model, prepared by Bertini,² which considers the formation of the compound nucleus and subsequent evaporation process to be preceded by the escape of cascade nucleons.

The primary proton flux through a slab shield can be calculated for the protons below 50 Mev in a typical flare spectrum; from this proton flux, the total neutron production spectrum as a function of energy and position can be found for each of the two reaction models. These neutrons will then be introduced as a source in the 05R neutron transport code (see Sect. 5.2). The resulting dose will be calculated as a function of depth in tissue for various shield thicknesses, and compared with the dose from secondary particles produced by the higher energy portion of the flare spectrum.

References

¹L. Dresner, *EVAP - A Fortran Program for Calculating the Evaporation of Various Particles from Excited Compound Nuclei*, ORNL-CF-61-12-30.

²H. Bertini, *Monte Carlo Calculations on Intranuclear Cascades*, ORNL-3383 (1963); see also *Phys. Rev.* **131**, 1801 (1963).

8.7. ERROR IN INTRANUCLEAR CASCADE CODE FOR INCIDENT PARTICLE ENERGIES FROM 25 TO 350 Mev

H. W. Bertini

Late in 1963 it was discovered that the intranuclear cascade code¹ for incident particle energies from 25 to 350 Mev contained an incorrect calculation of the location of the point of collision for the incident particles. The distance through nuclear matter for the first collision of the incident particle had been measured from a plane perpendicular to the incident particles and tangent to the

outer nuclear surface instead of from the point of intersection of the incident particle with the outer nuclear boundary as it should have been. The error did not, however, invalidate the conclusions in the results published in the open literature.² Its effect on almost all the data that were distributed was less than 20%.³

Figures 8.7.1–8.7.3 plot the uncorrected data along with the corrected data to illustrate some of the typical effects of the error. The corrected data are illustrated at only a few mass numbers. The difference between the corrected data and the uncorrected data is given by the difference between their corresponding values rather than between any lines drawn through the points.

References

¹Described by H. W. Bertini, *Neutron Phys. Div. Ann. Progr. Rept. Aug. 1, 1963*, ORNL-3499, Vol. II.

²H. W. Bertini, *Phys. Rev.* **131**, 1801 (1963).

³The author regrets any loss in time and effort that may have resulted from the use of the production data that were issued.

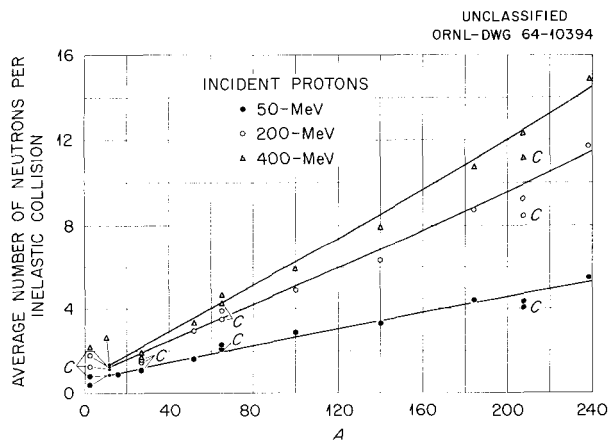


Fig. 8.7.1. Average Number of Emitted Cascade and Evaporation Neutrons per Inelastic Collision vs Mass Number A for Incident Protons. The C's indicate results from the corrected code and should be compared with the corresponding results from the uncorrected code rather than with the lines drawn through the points.

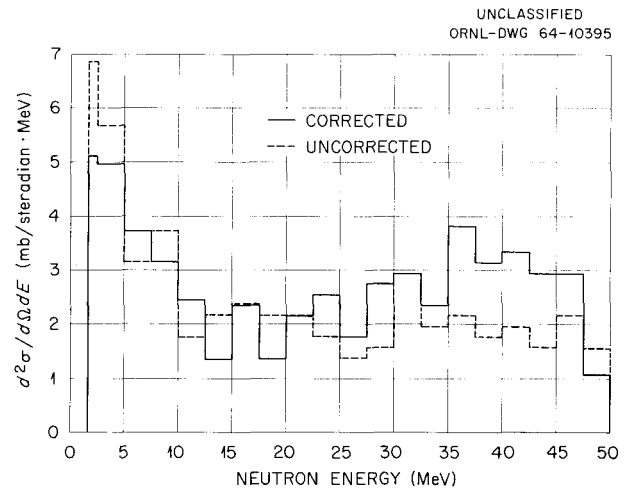


Fig. 8.7.2. Energy Spectra of Cascade Neutrons Emitted into the Laboratory Angular Interval 0 to 30° for 50-MeV Protons Incident on Aluminum.

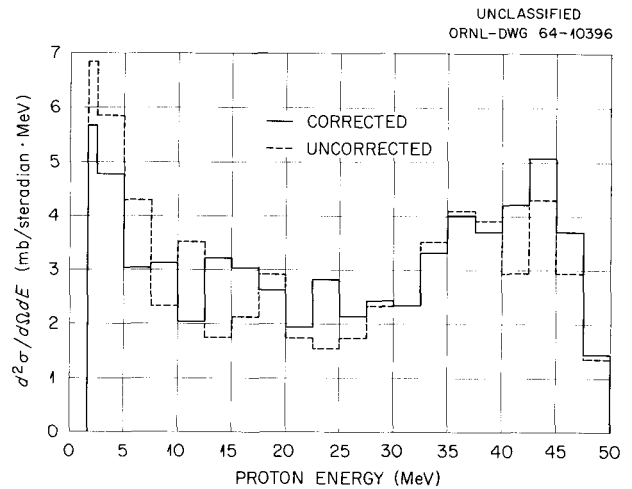


Fig. 8.7.3. Energy Spectra of Cascade Protons Emitted into the Laboratory Angular Interval 0 to 30° for 50-MeV Protons Incident on Aluminum.

8.8. INTRANUCLEAR CASCADE CALCULATIONS FOR INCIDENT PARTICLE ENERGIES FROM 25 MeV TO 2 GeV

H. W. Bertini

The intranuclear cascade calculation for incident particle energies from 25 MeV to 2 GeV previously reported¹ is undergoing debugging. The section

of the code pertaining to isobar formation has been "lifted" from the main code and will be completely debugged, and the angular distribution of the isobars (unknown at present) will be selected on the basis of comparisons with experimental data on particle-particle reactions.

In order to reduce coding errors, the entire program is being coded in FAP and FORTRAN by two different programmers. The results from each will be checked for consistency. The FORTRAN version will be the working version.

Preliminary results have been obtained from the FAP version, and some of the data are illustrated in Figs. 8.8.1 and 8.8.2 for 1-Gev protons incident on copper. Part of the output from the evaporation

code² used in the calculation is illustrated in Fig. 8.8.3 for this reaction. It is interesting to note the extent of the disintegration of the initial nucleus from such high-energy reactions. It must be stressed that these data are very preliminary inasmuch as this program has not yet been thoroughly checked.

In the previous annual report¹ mention was made of a problem concerning the treatment of pion production in potential fields: briefly, if the free-particle, four-component vector momentum (commonly referred to as "4-momentum") is used in the conservation laws for particle-particle reactions within the nucleus, then the nucleus can never be left with zero excitation energy if a pion

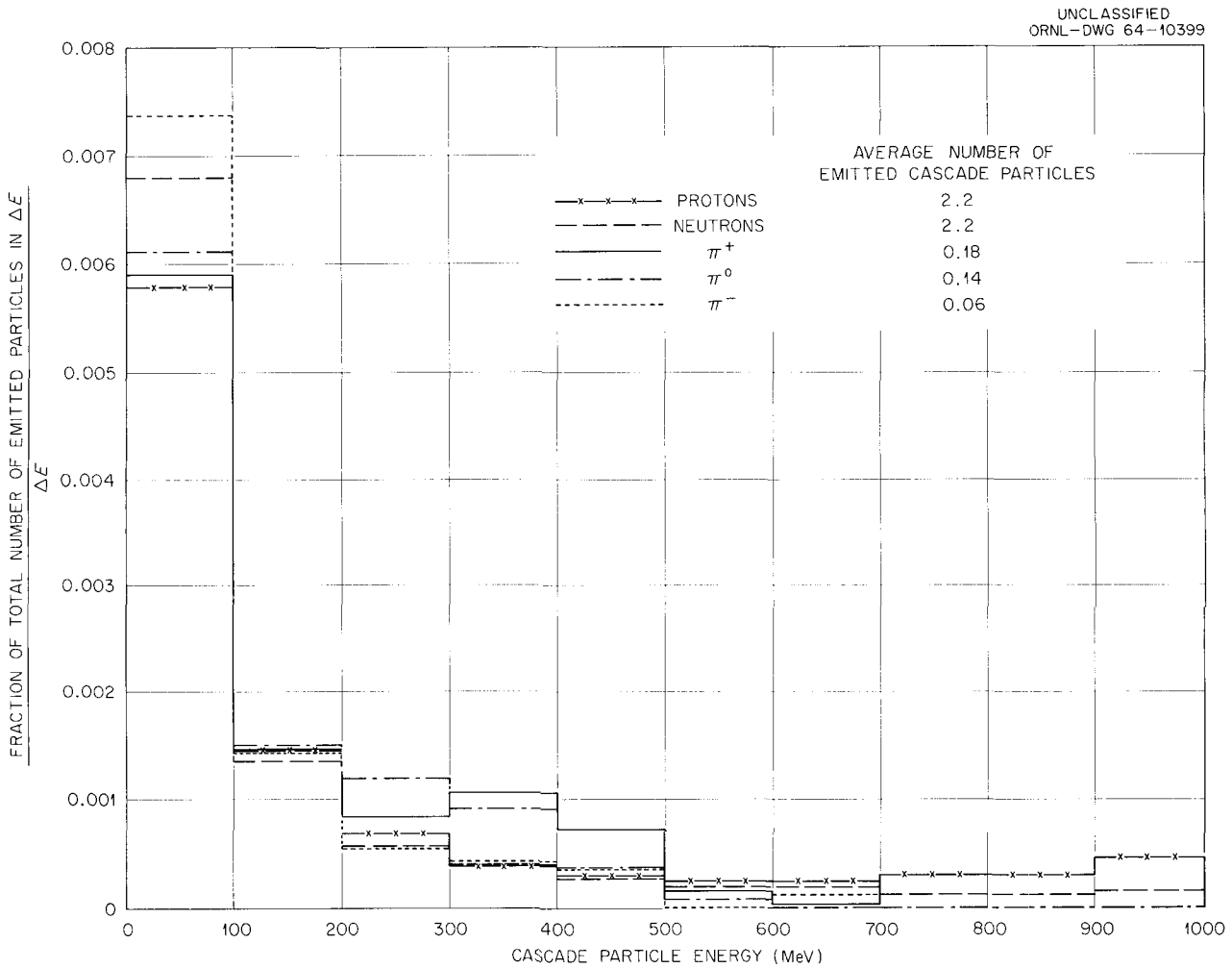


Fig. 8.8.1. Normalized Energy Spectra of Cascade Protons, Neutrons, π^+ , π^0 , and π^- Emitted in All Directions from 1-Gev. Protons Incident on Copper.

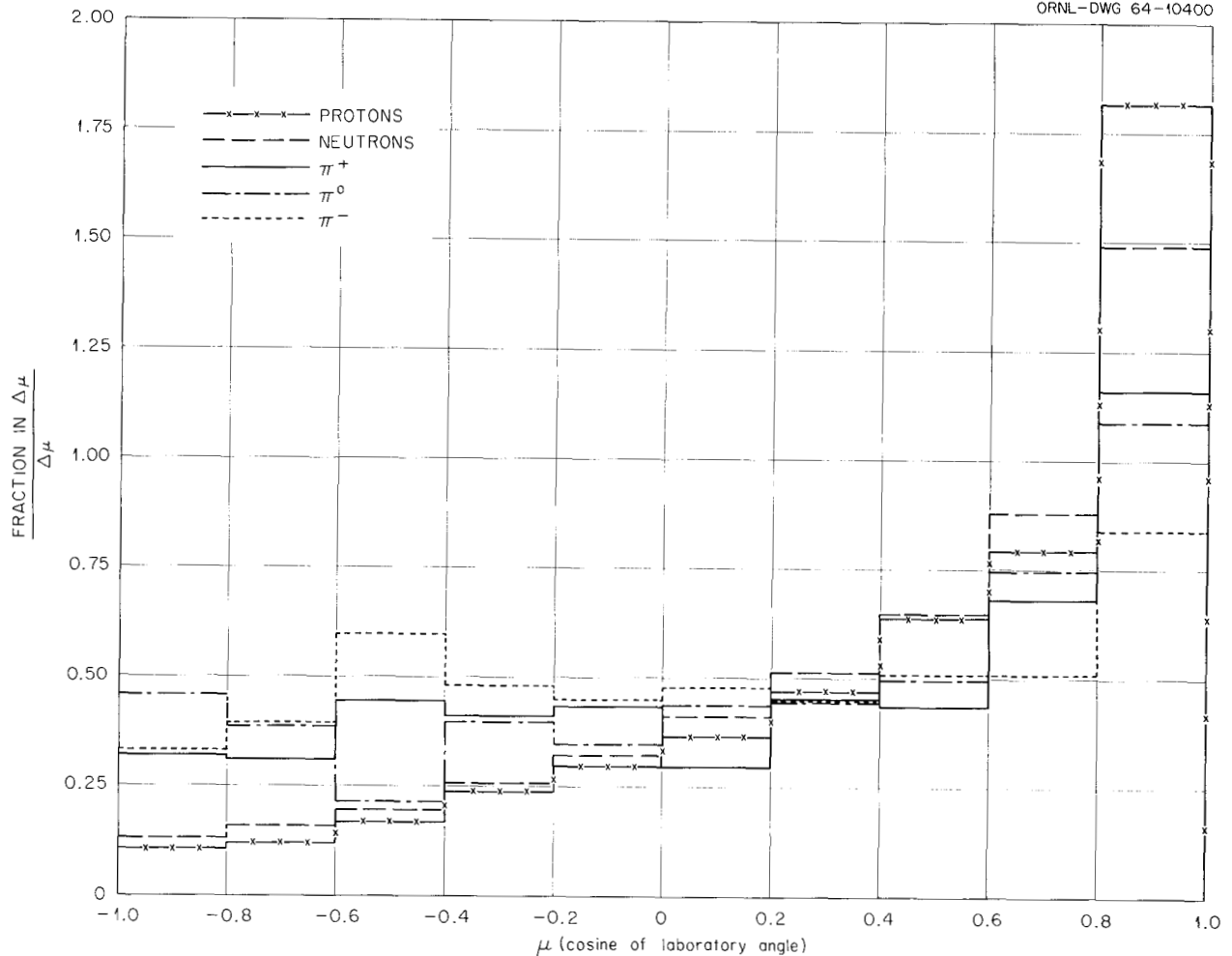


Fig. 8.8.2. Angular Distribution of Cascade Protons, Neutrons, π^+ , π^0 , and π^- of All Energies from 1-Gev Protons Incident on Copper.

is created in the particle-particle reaction. It was mentioned that the present version of the code uses the free-particle 4-momentum but that the kinetic energies of the decay products of the isobar formed in the creation process are arbitrarily increased by an amount $V/2$, where V is the depth of the potential, so that the nucleus can be left in a state of zero excitation energy. It was also mentioned that the difficulty could be removed by using a reduced mass, $m_r = m - V$, in the conservation equations, but to be consistent this mass should also be used in the equations governing simple scattering inside the nucleus.

The most rigorous approach to this problem would be to use a Lorentz invariant Lagrangian

for the reaction and derive the conservation theorems in a systematic fashion, using, for example, Hamilton's principle.³ Even if possible, however, such an approach would, in the opinion of many physicists of different specialties, be a very difficult task and the time involved would be prohibitive. Another approach, and the one used here, is to place restrictions on the forces involved and to accept the results that follow. If the restrictions are reasonable, the results will, hopefully, correspond to reality.

If the four-component vector force (4-force) is restricted to that whose space-like components are conservative and not explicitly dependent on the time and if the further restriction is added that

DISTRIBUTION OF RESIDUAL NUCLEI FOLLOWING EVAPORATION

A	Z	NUMBER OF NUCLEI	CROSS SECTION (MB)
30	15	10	2.92
	14	6	1.75
29	14	9	2.62
28	14	7	2.04
	13	1	0.29
27	14	1	0.29
	13	4	1.17
26	13	1	0.29
	12	1	0.29
25	12	3	0.87
24	12	3	0.87
23	11	2	0.58
22	11	1	0.29
	9	1	0.29
21	10	1	0.29
	9	2	0.58
20	8	1	0.29

Fig. 8.8.3. Sample Output Illustrating the Extent of the Disintegration of the Nucleus when Copper Is Bombed by 1-Gev Protons ($A = 65$, $Z = 29$). The page illustrated contains only the lightest of the residual nuclei calculated. The data for the heavier ones are contained on pages of output that are not shown. The column headed "Number of Nuclei" is the number remaining from 5000 incident particles.

the sum of the kinetic energy, rest energy, and potential energy be a constant of the motion, it can be shown that the rest mass must remain constant.

Using the notation of Rindler,⁴ the four components of the vector velocity, U^μ , are defined by

$$U^\mu = \frac{dX^\mu}{d\tau}, \quad (1)$$

where $d\tau$, the proper time, is defined as

$$d\tau^2 = -\frac{1}{c^2} (dx^2 + dy^2 + dz^2) + dt^2. \quad (2a)$$

For a particle of speed u

$$d\tau^2 = dt^2 \left[-\frac{1}{c^2} (dx^2 + dy^2 + dz^2) + 1 \right] \\ = dt^2 \left(1 - \frac{u^2}{c^2} \right) = \frac{dt^2}{\gamma^2}. \quad (2b)$$

Then

$$\frac{d}{d\tau} = \frac{dt}{d\tau} \frac{d}{dt} = \gamma \frac{d}{dt} \quad (3)$$

and

$$U^\mu = \frac{dX^\mu}{d\tau} = \gamma \frac{dX^\mu}{dt}. \quad (4)$$

The 4-vector U then has three components, given by $\gamma \bar{u}$, where \bar{u} is the 3-vector velocity and the fourth component of U is γc .

A 4-momentum with components P^μ is given by

$$P^\mu = m_0 U^\mu, \quad (5)$$

where m_0 is the proper (or rest) mass. Three of the components of P are $m_0 \bar{u} \gamma$, and the fourth is $m_0 \gamma c$.

One then defines a 4-force such that the components are given by

$$F^\mu = \frac{d}{d\tau} P^\mu = \gamma \frac{d}{dt} P^\mu, \quad (6)$$

with the space-like components given by

$$\gamma \frac{d}{dt} (m_0 \bar{u}) = \gamma \frac{d\bar{p}}{dt} = \gamma \bar{f}, \quad (7)$$

where \bar{f} is the 3-force. The time-like component of F^μ is $\gamma c [d(m_0 \gamma)/dt]$. If the differentiation implied in the definition is carried out,

$$F^\mu = \frac{d}{d\tau} P^\mu = \frac{d}{d\tau} (m_0 U^\mu) = m_0 \frac{dU^\mu}{d\tau} + U^\mu \frac{dm_0}{d\tau}, \quad (8)$$

and the scalar product $\hat{g}_{\nu\mu} U^\nu F^\mu$, where $\hat{g}_{\nu\mu}$ is the metric tensor, is taken, then

$$\hat{g}_{\nu\mu} U^\nu F^\mu = U_\mu F^\mu = m_0 U_\mu \frac{dU^\mu}{d\tau} + U_\mu U^\mu \frac{dm_0}{d\tau}. \quad (9)$$

To reduce each term on the right-hand side of Eq. (9), consider from the definition of $d\tau$,

$$\hat{g}_{\mu\nu} dX^\mu dX^\nu = c^2 d\tau^2.$$

Then

$$\hat{g}_{\mu\nu} \frac{dX^\mu}{d\tau} \frac{dX^\nu}{d\tau} = \hat{g}_{\mu\nu} U^\mu U^\nu = c^2. \quad (10)$$

Differentiating with respect to τ ,

$$\hat{g}_{\mu\nu} \frac{dU^\mu}{d\tau} U^\nu + \hat{g}_{\mu\nu} U^\mu \frac{dU^\nu}{d\tau} = 2U_\mu \frac{dU^\mu}{d\tau} = 0, \quad (11)$$

and the first term on the right-hand side of Eq. (9) vanishes.

Considering the second term of the right-hand side of Eq. (9), it follows from Eq. (10) that

$$U_\mu U^\mu = c^2.$$

Therefore the scalar product

$$\hat{g}_{\nu\mu} U^\nu F^\mu = U_\mu F^\mu = c^2 \frac{dm_0}{d\tau}. \quad (12)$$

It can be seen that the condition for a constant rest mass is that

$$U_\mu F^\mu = 0. \quad (13)$$

(All the above equations are given in ref. 4.)

Now using the first of our restrictions that the space-like components of the 4-force be conservative, that is, that a V exists such that $\bar{f} = -\bar{\nabla}V$, the vector F has components

$$F = \gamma \left[\bar{f}, c \frac{d}{dt} (m_0 \gamma) \right] = \gamma \left[-\bar{\nabla}V, c \frac{d}{dt} (m_0 \gamma) \right]. \quad (14)$$

The scalar product

$$U_\mu F^\mu = \gamma^2 \left[\bar{\nabla}V \cdot \bar{u} + c^2 \frac{d}{dt} (m_0 \gamma) \right]. \quad (15)$$

Then, with

$$\bar{\nabla}V \cdot \bar{u} = \frac{\partial V}{\partial x} \frac{dx}{dt} + \frac{\partial V}{\partial y} \frac{dy}{dt} + \frac{\partial V}{\partial z} \frac{dz}{dt},$$

it follows that

$$\bar{\nabla}V \cdot \bar{u} = \frac{dV}{dt} \quad (16)$$

provided that the second restriction, that V is not explicitly dependent on the time, applies, and

$$U_\mu F^\mu = \gamma^2 \left[\frac{d}{dt} (V + m_0 c^2 \gamma) \right]. \quad (17)$$

The quantity $V + m_0 c^2 \gamma$ represents the potential energy plus the rest mass energy plus the kinetic energy. If it is assumed that this sum is constant, then

$$U_\mu F^\mu = c^2 \frac{dm_0}{d\tau} = c^2 \gamma \frac{dm_0}{dt} = 0, \quad (18)$$

and therefore the rest mass is also a constant.

The weakness in this analysis is that the second restriction – that V is not an explicit function of the time – implies that the potential is not invariant to Lorentz transformations. In a moving frame of reference, V would be dependent on the time in general. However, in the frame of reference in which the cascade reactions are assumed to take place, the rest frame of the nucleus, these restrictions seem quite reasonable.

The alternative of using $m_r = m_0 - V$ has the effect of replacing the potential by a change in mass and carrying out all kinematics calculations with the reduced mass in place of the rest mass. In this form the potentials disappear, and a set of equations are obtained which are identical in form to the free-particle equations. But the fact

that the form of the equations is the same as that for free particles is simply insufficient to justify the correctness of that approach.

It would be interesting to compare the results of both approaches, but this cannot be done at this time; therefore the present version of the program will be continued.

References

¹H. W. Bertini, *Neutron Phys. Div. Ann. Progr. Rept. Aug. 1, 1963*, ORNL-3499, Vol. II, p. 27.

²H. W. Bertini, *Description of Printed Output from Intranuclear Cascade Calculation*, ORNL-3433 (May 14, 1963), p. 84.

³E. L. Hill, *Rev. Mod. Phys.* **23**, 253 (1951).

⁴W. Rindler, *Special Relativity*, Interscience, New York, 1960, p. 87.

8.9. RAPID COMPUTATION OF SPECIFIC ENERGY LOSSES FOR ENERGETIC CHARGED PARTICLES¹

R. W. Peelle

A method is demonstrated for computing rapidly in a digital computer the specific energy loss of energetic charged particles, excluding electrons. For energies larger than an empirically determined cutoff TLIM, the computation is based on use of the usual Bethe-Bloch equation with a "shell correction" for nonparticipation of tightly bound electrons in the absorber atoms, but without a "density effect" correction which might be required for incident proton energies as high as 1 Gev. Rapid computation is achieved by interpolating a combined "shell correction" from a small table of values stored with the set of parameters peculiar to a given absorber material. Accuracy is limited to a few tenths of a percent by the coarseness of the interpolation procedure and by the accuracy of the combined shell corrections presently available to serve as a base for interpolation. For incident energies less than TLIM, a plausible value is computed based wholly on a few empirical parameters. The results are compared with published tabulations of specific energy loss and with a very small selection of experiments on relative energy loss and range. A

computer subprogram which utilizes the described technique is listed in the IBM-7090 FORTRAN II language, and brief instructions for its use are given.

References

¹Abstract of ORNL TM-977 (in press).

8.10. ENERGY DEPOSITED BY HIGH-ENERGY ELECTRONS IN AN LiF OPTICAL SYSTEM OF THE ORBITING ASTRONOMICAL OBSERVATORY

H. S. Moran C. D. Zerby¹
F. C. Maienschein

The Orbiting Astronomical Observatory (OAO) is intended to provide an examination of the sky in the ultraviolet region, which is inaccessible from the surface of the earth. Lithium fluoride optical elements are used to transmit the ultraviolet, and since the satellite will approach the lower edge of the Van Allen radiation belt, a question arises concerning darkening of the LiF by the electrons in the belt.

The high-energy, three-dimensional, electron-photon cascade code² was used to determine the energy absorbed in the LiF optical elements in a slab approximation to the geometry of the orbiting telescope. The slabs were composed of 0.375-in.-thick titanium alloy (structure), 1.0-in.-thick fused quartz (mirror), 0.06-in.-thick LiF or quartz (filter), and, finally, 0.30-in.-thick LiF (lens). The energy deposited in each of these regions was calculated for electrons incident in the energy region from 1 to 6 Mev. As was pointed out in an earlier application of the code to a similar problem,³ the code is not particularly suitable for treating electrons below about 5 Mev because of the mathematical approximations which it contains. However, it was shown previously to give useful results and so is used again here to predict the energy absorbed due to both photons and electrons in the cascade. The energy absorbed due to the photons is negligible in all cases. Table 8.10.1 gives the energy deposited by the electrons for the case of an LiF filter.

Based on the calculated absorbed energies as shown in the table, together with the expected

Table 8.10.1. Energy Deposited by Electrons in the Slabs Used to Approximate the Geometry of the OAO

Incident Electron Energy (Mev)	Energy Deposited (Mev per Incident Particle)			
	In 0.375-in. Titanium Alloy	In 1.0-in. Quartz	In 0.06-in. LiF (Filter)	In 0.30-in. LiF
1.0	0.9564	0.0009	0.00001	0.00016
2.5	1.885	0.0074	0.0002	0.0013
3.0	2.821	0.0140	0.0004	0.0030
4.0	3.729	0.0281	0.0008	0.0061
6.0	5.500	0.0819	0.0019	0.0108

flux of electrons incident on the satellite and the measured radiation blackening of the LiF, it has been concluded by representatives of the OAO project that radiation blackening should not occur during the expected useful life of the telescope.

References

¹Union Carbide Research Institute, Tarrytown, N.Y.

²C. D. Zerby and H. S. Moran, *Neutron Phys. Div. Ann. Progr. Rept. Aug. 1, 1963*, ORNL-3499, Vol. II, p. 3.

³*Ibid.*, p. 12.

8.11. CALCULATION OF THE FLUX OF NEUTRONS DIFFUSING BENEATH THE SHIELD ("EARTHSHINE") OF A MESON FACTORY

W. E. Kinney

In a facility for producing mesons in copious quantities — a meson factory — protons of high energy (e.g., 800 Mev) impinge on a target and the mesons are produced as a result of intranuclear processes. Lower energy protons and neutrons also result from the nuclear interactions. All these secondary radiations present a hazard to personnel as well as to equipment, and adequate shielding must be provided. Approximate methods have been used to estimate the fluxes of secondaries coming through the shield,^{1,2} but apparently no such approximate method exists for estimating the flux

of neutrons which are born beneath the shield and diffuse into the experimental areas behind it, thus producing an "earthshine" analogous to skyshine. Accordingly, calculations are in progress to estimate the extent of the earthshine in an idealized configuration which, nevertheless, will be applicable to meson factory shields.

The idealized problem is illustrated in Fig. 8.11.1. An isotropic point source of 400-Mev neutrons is located at S, 5 ft above the surface of a semi-infinite medium of SiO₂ and 5 ft from the front face of an infinite slab of iron, 10 ft thick, resting on the earth. A nucleon transport code (Sect. 8.1) was used to start the neutrons at 400 Mev and to produce neutrons of energy less than 50 Mev as sources for the neutron transport code 05R (Sect. 5.2). To direct the neutrons into the most critical regions, they were strongly biased about the line SI in Fig. 8.11.1 and, if their directions carried them into the iron, they were permitted to pass through to the earth but with their

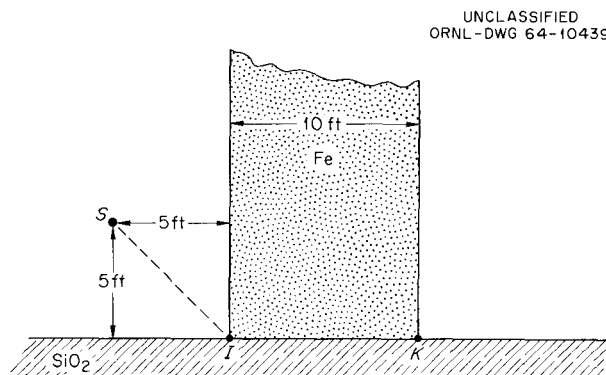


Fig. 8.11.1. An Idealized Meson Factory Shield.

weights reduced by the probability of traversing the iron. All secondaries above 50 Mev were also biased, toward point K. Finally, in order to save time, only neutrons which were born near (3–5 ft) point K were put into 05R, the contribution of the others being negligible. Two batches of 2000 neutrons were run through the high-energy transport, producing a total of 5466 and 5347 neutrons below 50 Mev. Of these, only 442 and 478 neutrons, respectively, lay within the permitted distance of point K.

Two independent runs were made on 05R for each of the groups of neutrons, giving a total of four runs on which preliminary results obtained by statistical estimation³ were based. The flux resulting from a unit source as a function of energy at a point on the earth surface 5 ft from the rear face of the shield is given in Table 8.11.1. It may be compared with an uncollided flux of 3.9×10^{-15} neutrons cm^{-2} (source neutron)⁻¹.

The average whole-body dose due to 400-Mev neutrons is roughly 5×10^{-8} rem (see Sect. 8.2), while the dose due to 1-Mev neutrons is about 3×10^{-8} rem (ref. 4), so that the hazard due to earthshine is approximately four orders of magnitude more severe than that from the direct beam.

Table 8.11.1. Flux as a Function of Energy
5 ft Behind the Shield on the Earth Surface

Energy Range (Mev)	Flux [neutrons cm^{-2} (source neutron) ⁻¹]
0.1–1	$(8.1 \pm 2.6) \times 10^{-11}$
1–2	$(7.9 \pm 5.6) \times 10^{-12}$
2–3	$(6.9 \pm 4.2) \times 10^{-13}$
3–4	$(1.1 \pm 0.9) \times 10^{-14}$
4–5	$(3.6 \pm 1.3) \times 10^{-15}$
5–6	$(3.5 \pm 2.0) \times 10^{-16}$
6–7	$(3.4 \pm 1.2) \times 10^{-15}$
7–8	$(2.6 \pm 1.4) \times 10^{-16}$
8–9	$(1.6 \pm 1.5) \times 10^{-14}$
9–10	$(2.9 \pm 0.9) \times 10^{-16}$
10–20	$(8.5 \pm 6.8) \times 10^{-15}$
20–30	$(5.1 \pm 4.2) \times 10^{-13}$
30–40	$(3.6 \pm 2.6) \times 10^{-17}$
40–50	$(1.3 \pm 1.3) \times 10^{-14}$

In an effort to reduce the variance, a smoothing of the 05R source data will be attempted so that a single neutron does not contribute so strongly for some batches and thus lead to large variances.

References

¹H. B. Knowles, p. 333 in *Minutes of the Conference on Proton Linear Accelerators Held at Yale University Oct. 21–25, 1963*, TID-7691.

²R. W. Wallace, *Nucl. Instr. Methods*, **18/19**, 405 (1962).

³W. E. Kinney, *Program STATEST, An Application of the Method of Statistical Estimation to the Calculation of Neutron Flux in Anisotropically Scattering Media by Monte Carlo*, ORNL-3715 (1964).

⁴“Protection Against Neutron Radiation up to 30 Million Electron Volts,” *National Bureau of Standards Handbook*, Vol. 63 (1957).

8.12. A SOLUTION TO THE NUCLEON-MESON CASCADE EQUATIONS UNDER VERY SPECIAL CONDITIONS¹

R. G. Alsmiller, Jr.

To check the numerical accuracy of cascade calculations, particularly the truncation error after calculating over very large distances, it is desirable to have analytic solutions to the equations for particular cases.

A variety of such solutions have been obtained previously under the assumption that the stopping power of all charged particles is zero.^{2,3} In this report the equations which describe a one-dimensional nucleon-meson cascade are solved under the following assumptions:

1. the secondary particle production kernels are taken to be of the special form

$$F_{ij}(E', E) = \alpha_i \gamma_j e^{\nu(E' - E)} \quad \text{for all } i, j,$$

$$\alpha_i, \gamma_j, \nu = \text{constant};$$

2. pion decay is neglected;
3. pion and nucleon nonelastic cross sections are taken to be constant;
4. the stopping powers of all charged particles are equal to the same nonzero constant.

References

¹Abstract of ORNL-3570 (in press).

²C. Passow, Deutsches Elektronen-Synchrotron, Hamburg, Germany, *Phenomenologische Theorie Zur Berechnung einer Kaskade aus Schweren Teilchen (Nukleonkaskade) in der Materie*, Desy-Notiz A. 285 (February 1964).

³F. S. Alsmiller and R. G. Alsmiller, Jr., *Neutron Phys. Space Radiation Shielding Research Ann. Progr. Rept. Aug. 31, 1962*, ORNL-CF-62-10-29, p. 138.

8.13. NUMERICAL SOLUTIONS OF THE ONE-DIMENSIONAL NUCLEON-MESON CASCADE EQUATIONS¹

R. G. Alsmiller, Jr. J. E. Murphy²
J. Barish³

In shielding calculations for high-energy accelerators, it is necessary to solve the nucleon-meson cascade equations numerically for very large distances. The calculations are quite extensive

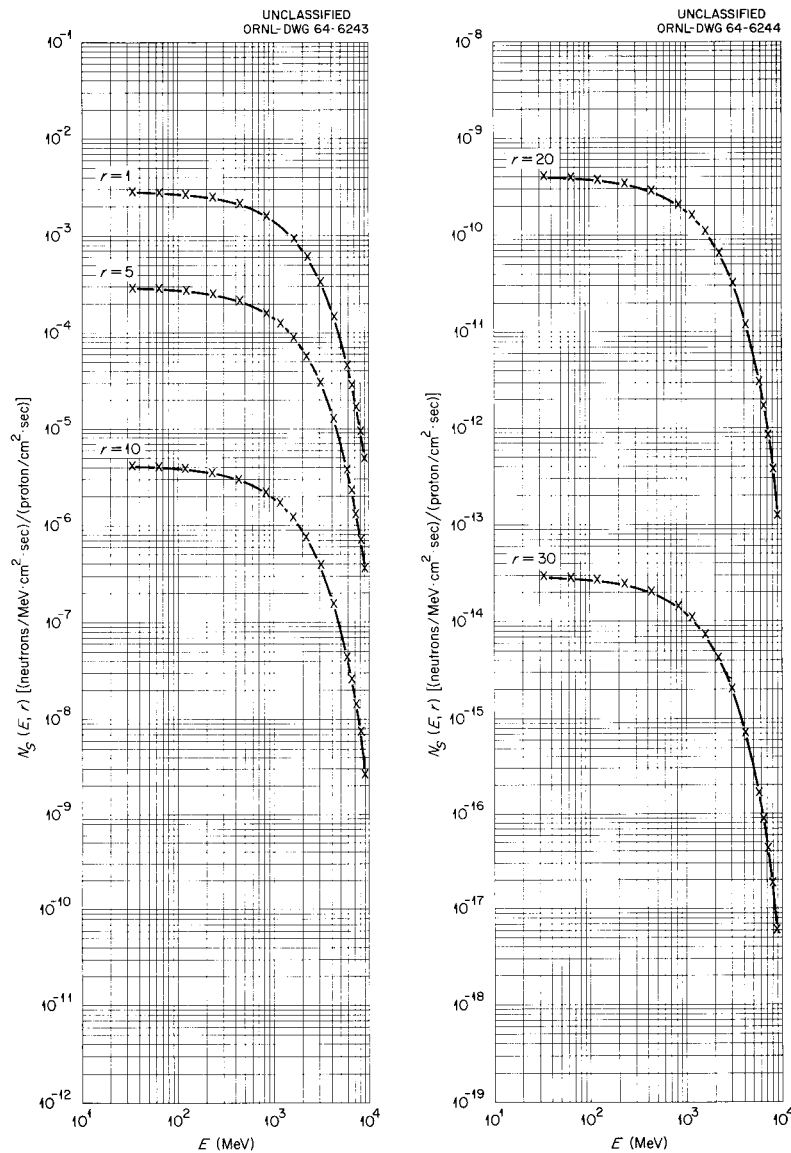


Fig. 8.13.1. Secondary Neutron Flux vs Energy ($E_0 = 10$ Gev). Curve, numerical solution; points, analytic solution; r is measured in collision lengths ($= 93$ g/cm²).

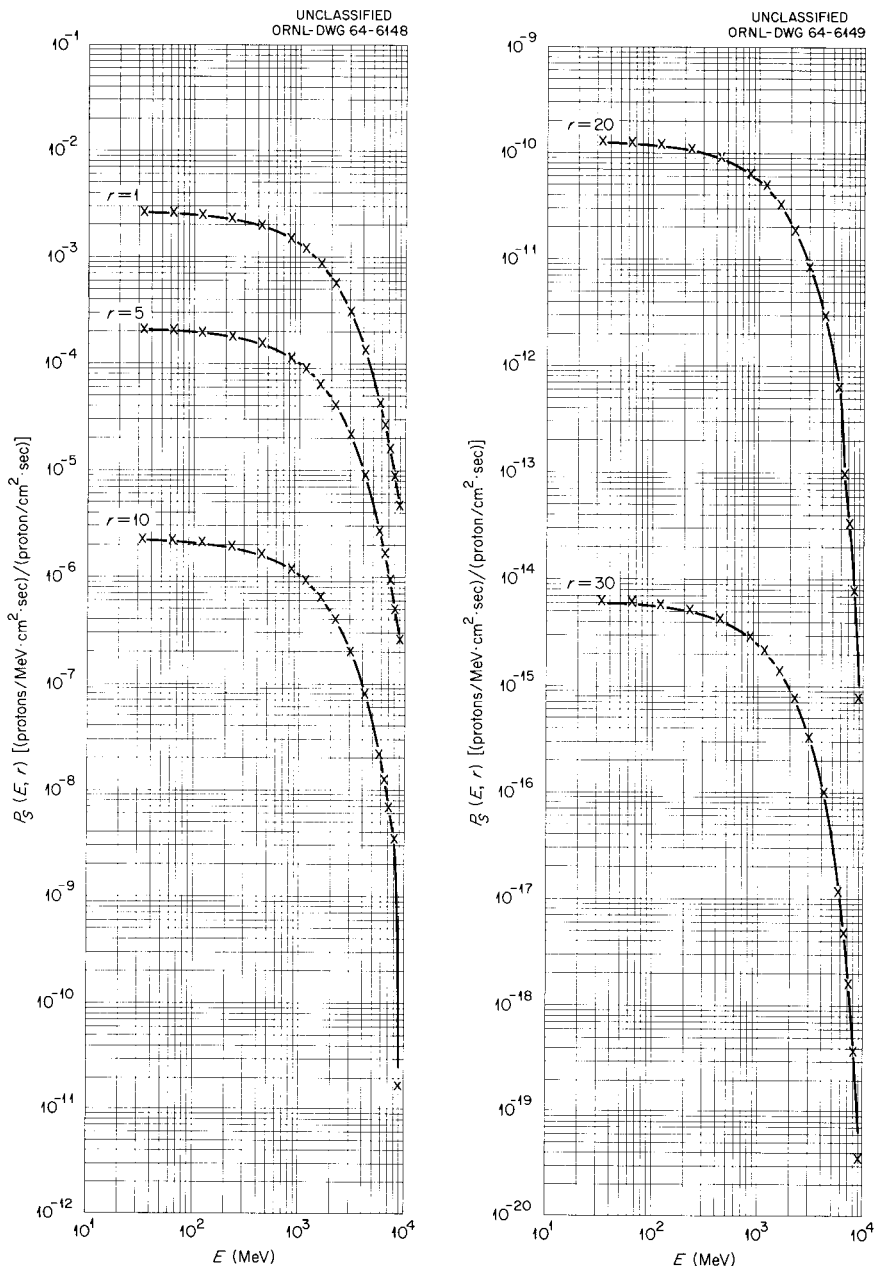


Fig. 8.13.2. Secondary Proton Flux vs Energy ($E_0 = 10$ Gev). Curve, numerical solution; points, analytic solution; r is measured in collision lengths ($= 93.8 \text{ g/cm}^2$).

and the truncation error could be excessive. For the case of a 10-GeV proton beam and a set of quite special physical assumptions, an analytic (quadrature) solution to the cascade equations has been obtained (Sect. 8.12), and the results have been compared with those from a numerical solution.

The calculation of the primary flux for this case is quite trivial, and the two calculations give, for all practical purposes, the same result. Figure 8.13.1 shows the secondary neutron flux as a function of energy for various r values, and Fig. 8.13.2 shows the secondary proton flux as a function of energy. The solid curves represent

the numerical solution, while the plotted points represent the analytic solution. Because of the manner in which the constants were chosen, the comparison of the pion fluxes is exactly the same as the comparison of the proton fluxes.

The two solutions are in excellent agreement at all energies and at r values up to 30 mean free paths (~ 2800 g/cm²). At very high energies (all curves go to zero at 10 Gev) the numerical solution for the proton flux tends to be slightly higher than the analytic solution, but since the spectrum is decreasing so rapidly at these energies the error is of no practical importance.

References

¹Summary of ORNL-TM-951 (September 1964).

²Present address: Arthur D. Little Co., Boston, Mass.

³Central Data Processing Facility of Oak Ridge Gaseous Diffusion Plant.

8.14. NUCLEON-MESON CASCADE CALCULATIONS: TRANSVERSE SHIELDING FOR A 45-GeV ELECTRON ACCELERATOR (PART IV)¹

R. G. Alsmiller, Jr. F. S. Alsmiller
J. Barish²

In a series of previous reports³ nucleon-meson cascade calculations were carried out for several cases of interest in the design of the transverse shield for the proposed 45-GeV linear electron accelerator at Stanford University. Since these reports were written the IBM code with which the calculations were done has been rewritten and includes a variety of numerical improvements. Furthermore, the production of mesons from pion decay is treated more correctly in the present code than in the previous one.

To test the validity of the previous work, one of the cases considered in ref. 3 has been recalculated, with the same physical data and initial values that were used in ref. 3. There are some numerical differences between the present and previous results, but the total dose estimates obtained from the two calculations are essentially the same.

References

¹Abstract of ORNL-3734 (in press).

²Central Data Processing Facility of the Oak Ridge Gaseous Diffusion Plant.

³R. G. Alsmiller, Jr., F. S. Alsmiller, and J. E. Murphy, *Nucleon-Meson Cascade Calculations: Transverse Shielding for a 45-GeV Electron Accelerator. Part I*, ORNL-3289 (1962); *Part II*, ORNL-3365 (1962); *Part III*, ORNL-3412 (1963).

8.15. ANALYTIC SOLUTIONS TO NUCLEON-MESON CASCADE EQUATIONS FOR SPECIAL CASES OF SECONDARY PARTICLE PRODUCTION KERNELS¹

F. S. Alsmiller

Solutions in quadrature have been obtained for some coupled one-dimensional nucleon-meson cascade equations in the absence of pion decay and charged-particle stopping. Absorption cross sections are assumed to have the same constant value for all particles. These restrictions limit the value of the solutions to cases of relatively high energy and dense media.

The cross sections, $F_{jk}(E, E')$, for the production of secondary particles of type j and energy E by particles of type k and energy E' in nonelastic collisions are taken to be of two general forms:

$$F_{jk}(E, E') = \frac{g_k(E')}{g_j(E)} [K_j(E, E') + h(E)k(E')\delta_{jk}] ; \quad (1)$$

where

$$\sum_j K_j(E, E') + h(E)k(E') = H(E)L(E') ;$$

and

$$F_{jk}(E, E') = \frac{g_k(E')}{E'g_j(E)} \left\{ a_j + b_j \left(\frac{E'}{E} \right)^\eta + c_j \left(\frac{E'}{E} \right)^\gamma + \delta_{jk} \left[a_0 + b_0 \left(\frac{E'}{E} \right)^\eta + c_0 \left(\frac{E'}{E} \right)^\gamma \right] \right\} ; \quad (2)$$

where η , γ , a_j , b_j , c_j , a_0 , b_0 , and c_0 are arbitrary constants; and g_k , g_L , h , k , H , and L are arbitrary functions. Some examples of Eq. (1) are given.

References

¹Abstract of ORNL-3746 (to be published).

8.16. STATISTICAL MODEL CALCULATIONS OF NUCLEON-NUCLEON AND PION-NUCLEON COLLISIONS: CENTER-OF-MASS SPECTRA¹

R. G. Alsmiller, Jr.

In order to consider nucleon-nucleus and pion-nucleus collisions, it is necessary to know in detail the results of nucleon-nucleon and pion-nucleon collisions. In the energy region where multiple pion production is possible, sufficiently detailed experimental information is not available; thus it is necessary to use theoretical models to obtain the required information.

Calculations for nucleon-nucleon and pion-nucleon collisions based on the statistical model have been carried out.^{2,3} The calculations were done with an IBM code written by D. J. Jones⁴ at CERN and are, in principle, no different from a variety of such calculations carried out previously.⁵

In the calculations strange-particle production was neglected and no charge analysis was performed; that is, results were obtained only after summing over all charge components of a particular kind of particle. The center-of-mass energy spectra (averaged over all center-of-mass angles) and the multiplicities of nucleons and pions were obtained for a variety of cases with laboratory energies in the range 0.8 to 10 Gev.

References

¹Abstract of ORNL-3713 (in press).

²R. Hagedorn, *Nuovo Cimento* **15**, 434 (1960).

³M. Kretzschma, *Ann. Rev. Nucl. Sci.* **2**, 1 (1961).

⁴D. J. Jones, *Two Programmes for the IBM 709 Computer to Calculate Multiple Phase Space Integrals and High Energy Particle Production*, CERN-63-1 (Jan. 16, 1963).

⁵An extensive list of references to previous calculations is given by Hagedorn (ref. 2) and by Kretzschma (ref. 3).

8.17. STATISTICAL MODEL CALCULATIONS OF NUCLEON-NUCLEON AND PION-NUCLEON COLLISIONS: LABORATORY ENERGY-ANGLE DISTRIBUTIONS ASSUMING ISOTROPY IN THE CENTER-OF-MASS SYSTEM¹

R. G. Alsmiller, Jr.

Section 8.16 (abstract of ORNL-3713) discusses statistical model calculations that were carried out for nucleon-nucleon and pion-nucleon collisions, the results of which were reported for the center-of-mass spectra of both pions and nucleons. If the results of ORNL-3713 are to be usable in studying nucleon-nucleus and pion-nucleus collisions, it is necessary that they be transformed into the laboratory system. This transformation requires a knowledge of the angular distribution of the particles in the c.m. system. The statistical model, however, gives no information concerning these angular distributions (all results in ORNL-3713 are averaged over c.m. angles). Therefore it is necessary to introduce an assumption about these angular distributions before carrying out the transformation.

For present purposes — obtaining results which may be used in studying nucleon-nucleus and pion-nucleus collisions — the transformation has been carried out on the assumption that all particles, both nucleons and pions, are isotropically distributed in the c.m. system. Calculations have been carried out for all cases for which center-of-mass spectra were given in ORNL-3713.

References

¹Abstract of ORNL-3716 (in press).

8.18. NUCLEON-NUCLEUS AND PION-NUCLEUS COLLISIONS IN THE ENERGY RANGE 2 TO 10 Gev

R. G. Alsmiller, Jr.

Major uncertainties in shielding calculations for high-energy accelerators arise from lack of information concerning nucleon-nucleus and pion-nucleus collisions. To partially alleviate this difficulty, approximate calculations of the results of such collisions are being performed.

The data concerning nucleon-nucleon and pion-nucleon elastic collisions which are needed in the nuclear calculations have been obtained from experimental measurements. The energy distributions and multiplicities from nucleon-nucleon and pion-nucleon inelastic collisions have been obtained from a Fermi statistical model (see Sect. 8.16, abstract of ORNL-3713, and Sect. 8.17, abstract of ORNL-3716). This information is being used in intranuclear cascade calculations carried out in a one-dimensional approximation, that is, under the assumption that all particles are emitted in the direction of the incident particle. This means, of course, that no information concerning the angular distributions of the emitted particles will be obtained. Furthermore, the Fermi momentum of nucleons in the nucleus is neglected and pion absorption by two nucleons is neglected; so the energy distributions of the emitted particles will be obtained only at relatively high energies ($\gtrsim 500$ Mev).

For simplicity, the statistical model was used to obtain only nucleon and pion energy distributions rather than an explicit energy distribution for each charge state. Therefore the nuclear cascade calculations will yield only nucleon and pion distributions.

After the cascade calculations are performed, the results will be averaged over distance to simulate the collision between the incident particle and a spherical nucleus. In this averaging process a spatial variation of the density distribution of nucleons in the nucleus will be included.

8.19. PAIR PRODUCTION CROSS-SECTION PROGRAM

C. D. Zerby¹ C. W. Nestor, Jr.²

A program for the CDC-1604 computer has been written and is now in operation to compute the differential cross section for the production of a pair of Dirac particles by photons in the unscreened Coulomb field of a nucleus. Input to the program consists of the incident photon energy, in Mev, the fraction of the available kinetic energy carried by one member of the pair, and the maximum angular momentum to be included in calculating the cross sections. Output from the program consists of the coefficients of the Legendre polynomial expansion

of the cross section. The method used is essentially that of Jaeger and Hulme.³ Our program is designed to allow for higher angular momenta and higher incident energies than those used by Jaeger and Hulme.

To date the results show that total cross sections calculated by the program are in good agreement for materials with low atomic number with values calculated from the Born approximation formula of Bethe and Heitler.⁴ Work is under way on a calculation of differential cross sections by the Born approximation to provide an additional check on the results of the computer calculations.

References

¹Union Carbide Research Institute, Tarrytown, N.Y.

²Mathematics Division.

³J. C. Jaeger and H. R. Hulme, *Proc. Roy. Soc. (London)* **A153**, 443 (1936).

⁴H. A. Bethe and W. Heitler, *Proc. Roy. Soc. (London)* **A146**, 83 (1934).

8.20. STATISTICAL FLUCTUATIONS IN THE OUTPUT OF AN INTRANUCLEAR CASCADE MONTE CARLO COMPUTATION¹

R. W. Peelle

An effort has been made to estimate the magnitude of the statistical fluctuations in the differential secondary-nucleon cross-section output by the Bertini intranuclear cascade computation and to compare these estimates to the scatter observed between successive Monte Carlo outputs. Poisson statistics are found to be adequate to explain the fluctuations in the number of outgoing particles estimated for small energy and angle ranges. A chi-square test with one degree of freedom was performed for each energy and angle bin, and both the distribution of these values and the combined chi-square test confirm the reasonableness of the estimated variances. To explain the fluctuations in the output of the associated nucleon evaporation program, it is necessary to employ variance estimates based on a binomial approximation. A complete statistical analysis of the problem is not performed.

References

¹Abstract of ORNL-TM-771 (January 1964).

**8.21. DIFFERENTIAL BREMSSTRAHLUNG
CROSS SECTIONS FOR LOW-ENERGY
ELECTRONS¹**

J. D. Lawson²

Bremsstrahlung cross sections have been calculated for screened and nonscreened targets for electrons with energies from 0.05 to 5 Mev. The cross sections were obtained by numerical integration of the Bethe-Heitler equation for bremsstrahlung cross sections which are differential in photon energy and in photon and electron emission angles. Values of the bremsstrahlung cross sections which are differential in photon energy and doubly differential in photon energy and photon emission angle are tabulated.

References

¹Abstract of ORNL-TM-790 (February 1964).

²ORINS Fellow, Summer 1963.

**8.22. SPACE VEHICLE SHIELDING STUDIES
(PART III): THE ATTENUATION OF
A PARTICULAR SOLAR FLARE
BY AN ALUMINUM SHIELD¹**

R. G. Alsmiller, Jr. J. E. Murphy²

Using the straightahead approximation, nucleon-meson cascade calculations have been carried out for a particular solar-flare proton spectrum incident on a shield. The shielding material has approximately the properties of aluminum. Both spherical-shell and slab geometries were considered.

References

¹Abstract of ORNL-3549 (November 1963).

²Present address: Arthur D. Little Co., Boston, Mass.

9. Experimental Studies for High-Energy Radiation Shielding

9.1. THE SPACE, TIME, AND ENERGY DISTRIBUTIONS OF THE PROTON BEAM OF THE HARVARD UNIVERSITY SYNCHROCYCLOTRON¹

R. T. Santoro

The space, time, and energy distributions of the proton beam of the Harvard University Synchrocyclotron were measured. The spatial distribution was estimated from multiple-scattering approximations and measured by means of x-ray films and a beam-profile counter telescope. Experimental results may be approximated by a Gaussian function with $\sigma = \pm 0.28$ cm, with agreement between the observed results and the multiple-scattering estimates being favorable. Ninety-eight percent of the protons were contained in an 0.84-cm beam radius. Analysis of the macroburst structure revealed a gross duty cycle of $(4 \pm 2)\%$, depending on proton injection and extraction parameters. Oscilloscope observations of the microstructure showed that the proton bursts occurred at regular 42-nsec intervals, with the width of the time distribution of protons being less than 7 nsec. The standard deviation of the time between adjacent bursts of protons was measured to be 1.4 nsec by a delayed-coincidence technique.

The proton beam energy was determined from measurements of the proton range in copper and from time-of-flight measurements. The beam energy determined from the range measurements was 160.3 ± 0.6 Mev. The rms range spread was measured from the differential range curve as 0.34 ± 0.05 g/cm², which may be compared with the calculated straggling standard deviation of 0.32 g/cm². The proton energy measured by flight-time analysis over a 355-cm flight path was 153.38 ± 4.1 Mev.

References

¹Abstract of ORNL-3722 (in press).

9.2. MEASUREMENT OF THE INTENSITY OF THE PROTON BEAM OF THE HARVARD UNIVERSITY SYNCHROCYCLOTRON FOR ENERGY-SPECTRAL MEASUREMENTS OF NUCLEAR SECONDARIES¹

R. T. Santoro R. W. Peelle

Two thin helium-filled parallel-plate ionization chambers were designed for use in continuously monitoring the 160-Mev proton beam of the Harvard University Synchrocyclotron over an intensity range from 10^5 to 10^{10} protons/sec. The data were required for support of various measurements of energy spectra of neutrons, protons, and gamma rays resulting from the interaction of high-energy protons with various targets representative of typical space vehicle shielding materials.

The ionization chambers were calibrated by two independent methods. In four calibrations the charge collected in the ionization chambers was compared with that deposited in a Faraday cup which followed the ionization chambers in the proton beam. In a second method a calibration was made by individually counting beam protons with a pair of thin scintillation detectors. The ionization chamber response was found to be flat within 2% for a five-decade range of beam intensity.

Comparison of the Faraday-cup calibrations with that from proton counting shows agreement to within 5%, which is considered satisfactory for the uses to which the data will be put. The

experimental results were also in agreement, within estimated errors, with the ionization chamber response calculated by using an accepted value of the average energy loss per ion pair for helium. A slow shift in the calibrations with time is ascribed to a gradual contamination of the helium in the chambers by air leakage.

An appendix describes the calibration of standard current sources used for accurate calibration of the current-measuring instruments.

References

¹Abstract of ORNL-3505 (March 1964).

9.3. SPECTRA OF GAMMA RAYS PRODUCED BY THE INTERACTION OF ~ 160 -Mev PROTONS WITH Be, C, O, Al, Co, AND Bi¹

W. Zobel F. C. Maienschein
R. J. Scroggs²

A measurement of the gamma rays in the energy range 0.6 to 11 Mev resulting from bombardment of Be, C, H₂O, Al, Co, and Bi targets with ~ 160 -Mev protons has been completed. A three-crystal scintillation spectrometer was used as a pair spectrometer for photons having energies above 2 Mev and as a total-absorption, anticoincidence spectrometer for photons having energies below 2.5 Mev. A time-of-flight method was used to reject counts due to neutrons, with an average rejection efficiency of 0.70 ± 0.01 . Data were obtained in the form of pulse-height spectra, which were converted to photon spectra by a computer-programmed "unscrambling" technique; this technique resulted in the assignment of upper and lower spectral bounds which represented a 68% confidence interval. The bulk of the data was obtained at 136° from the direction of the proton beam; data obtained with Al targets at 44° and 20.5° give no evidence of anisotropy.

Discrete gamma rays were found for all materials except Bi. Cross sections for the production of these gamma rays were computed, and plausible assignments were made for the transitions giving rise to these lines. In the case of Al, Co, and Bi a continuum was observed, underlying the discrete spectrum for the Al and Co targets.

The total gamma-ray production cross sections for photons in the energy range 0.6 to 11 Mev were calculated to be the following: Be, 6.8 ± 1.3 mb; C, 41.4 ± 6.3 mb; O, 115 ± 22 mb; Al, 434 ± 97 mb; and Co, 1050 ± 220 mb. Where comparisons with the work of other investigators are available, the present cross-section results appear to be, in general, somewhat larger.

References

¹Abstract of ORNL-3506 (in press).

²Present address: Oak Ridge Technical Enterprises Corp., Oak Ridge.

9.4. DIFFERENTIAL CROSS SECTIONS BY FLIGHT-TIME SPECTROSCOPY FOR PROTON PRODUCTION IN REACTIONS OF 160-Mev PROTONS WITH VARIOUS NUCLEI

R. W. Peelle N. W. Hill¹
T. A. Love R. T. Santoro

Flight-time spectroscopy was employed to measure differential cross sections for the production of secondary protons in several elements by 160-Mev incident protons from the Harvard University Synchrocyclotron. The results of this experiment, which was subsidiary to one in which cross sections for secondary neutron production were measured, have been compared with the Monte Carlo cascade and evaporation predictions of Bertini² and Dresner,³ with some comparisons including the effects of instrument smearing. The results have also been compared with those from related experimental work (Sect. 9.5), and, in cases where they are directly comparable, the data are in agreement.

The equipment and some preliminary results were described previously.⁴ A cyclotron average current of about 5×10^4 protons/sec was employed; so two protons were observed in the same rf acceleration cycle only 1/25 of the time. Therefore a scintillator telescope placed in the beam ahead of the ~ 0.6 -g/cm²-thick targets served to announce zero flight time for each beam proton and allowed a count of the usable ones. The scintillator telescope used to detect scattered charged particles was too thick for

protons having energies <20 Mev, and could not discriminate among the possible kinds of charged secondaries. Flight-time resolution was about 1 nsec, providing energy resolution of about 20% at 45 Mev for the 90-cm-long flight path commonly used. At energies below 30 Mev, target thickness dominated the energy resolution.

The raw data showed that target-out backgrounds were not severe but that timing resolution and drift were serious problems. At low energies time channels were combined into bins of width gaged by the energy resolution. The response of each bin as a function of scattered proton energy was computed by carefully summing contributions over the target, taking into account energy-loss and flight-time increments in each of the eight materials through which the secondary protons passed, as well as the time resolution of the system and its time slewing as a function of pulse height. Uncertainties in these and other experimental parameters were propagated to the final cross sections. The angular smearing induced by multiple Coulomb scattering was less than the $6-8^\circ$ resolution given by the detector size, except at low energies for the cobalt and bismuth targets.

Table 9.4.1 gives the integrated cross sections, $\sigma(\theta, E' > 20 \text{ Mev})$, for the production of secondary protons having energies above 20 Mev. The calculated values are from the intranuclear cascade Monte Carlo estimates. Although measurements were made for a scattering angle of 10° , no values are given because the integrated cross sections there are dominated by elastic scattering. Figure 9.4.1 shows the smoothly changing results observed at 30° for targets ranging in mass number from 9 to 209.

The general energy dependence of the differential cross sections determined experimentally is consistent with that suggested by the intranuclear cascade estimates. At scattering angles $\geq 90^\circ$ the sharp cutoff with energy appears to occur at too low an energy in the computations, and at small angles the quasi-elastic peak is not defined as well by the experimental data as by the Monte Carlo work. When the computed results were smeared by the computed instrument response these differences continued to exist. Figure 9.4.2 illustrates this trend for proton production from cobalt at 30° . At 10° for aluminum

and cobalt, the computations give inadequate intensities by factors of 3 and 1.8, respectively, in the 20- to 50-Mev region, where detection of the inelastic events is not confused by strong elastic scattering.

Table 9.4.1. Laboratory System Angle-Differential Cross Sections for the Production of Secondary Protons of Energy >20 Mev

Target	Integrated Cross Section (mb/steradian)	
	Experimental	Calculated
Scattering Angle = 30° ($24-35^\circ$) ^a		
H ₂ O	152 ± 7	128 ± 4 ^b
D ₂ O	157 ± 7	102 + x ^c
Be	70 ± 2	70 ± 2
C	75 ± 2	87 ± 3
Al	124 ± 4	125 ± 3
Co	187 ± 7	(188 ± 5) + 0.7 ^d
Bi	330 ± 14 ^e	254 ± 7
Scattering Angle = 45° ($40-50^\circ$) ^a		
Al	80 ± 3	85 ± 2
Co	129 ± 5	(129 ± 3) + 1.8 ^d
Scattering Angle = 60° ($56-64^\circ$) ^a		
H ₂ O	54 ± 3	47 ± 2 ^f
Al	43 ± 1.5	45 ± 2
Co	70 ± 3	(67 ± 3) + 1.8 ^d
Scattering Angle = 90° ($85-95^\circ$) ^a		
Al	11.4 ± 0.6	8.0 ± 0.7
Co	21.2 ± 1.1	(12.5 ± 0.9) + 1.4 ^d
Scattering Angle = 120° ($110-131^\circ$) ^a		
Co	9.7 ± 0.7	(2.5 ± 3) + 1.5 ^d

^aValues in parentheses give the angular interval for the calculation.

^bA contribution of 26 mb/steradian is included for hydrogen scattering.

^cx is the unknown contribution from scattering in deuterium.

^dThis is a contribution predicted from the evaporation proton spectrum smeared by the instrument response.

^eEstimated contribution from elastic scattering is less than 10 mb/steradian.

^fA contribution of 15 mb/steradian is included for hydrogen scattering.

References

- ¹Instrumentation and Controls Division.
²H. W. Bertini, *Phys. Rev.* **131**, 1801 (1963).
³L. Dresner, *EVAP, A FORTRAN Program for Calculating the Evaporation of Various Particles from Excited Compound Nuclei*, ORNL-CF-61-12-30 (December 1961).
⁴R. W. Peelle *et al.*, *Neutron Phys. Div. Ann. Progr. Rept. Aug. 1, 1963*, ORNL-3499, Vol. II, p. 73.

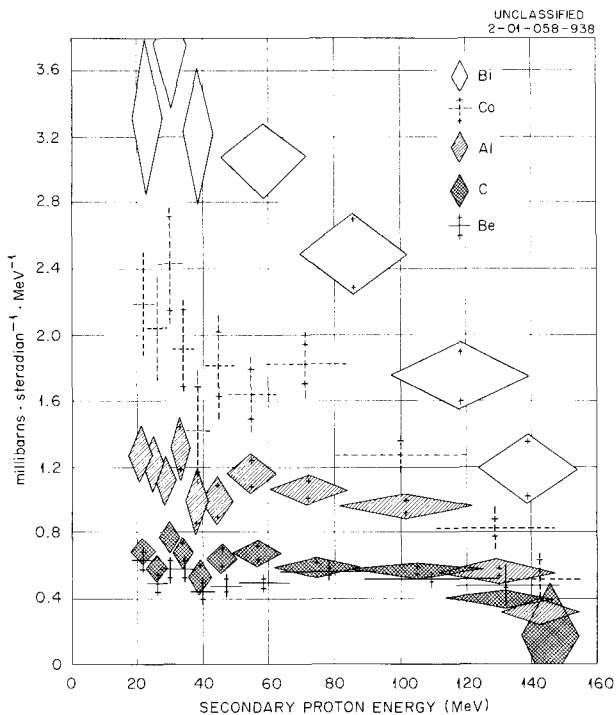


Fig. 9.4.1. Cross Sections for the Production of Secondary Protons at 30° by 160-Mev Protons Incident on Targets of Bi, Co, Al, and C, as a Function of Secondary Proton Energy.

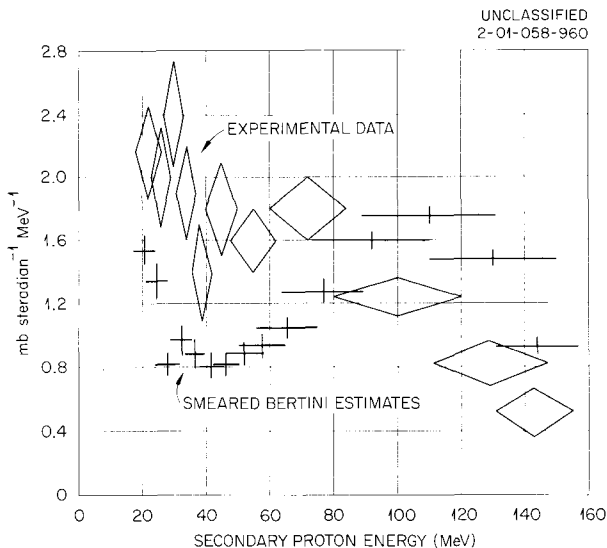


Fig. 9.4.2. Experimental and Theoretical Cross Sections for the Production of Secondary Protons at 30° by 160-Mev Protons Incident on Co, as a Function of Secondary Proton Energy.

9.5. SPECTRA OF NEUTRONS AND PROTONS FROM TARGETS BOMBARDED BY 160-Mev PROTONS

J. W. Wachter W. R. Burrus
 W. A. Gibson C. F. Johnson¹

A proton spectrometer has been used to measure secondary neutron and proton spectra from targets bombarded by 160-Mev protons. The spectrometer consists of three scintillation counters, operated in coincidence to define the angle of acceptance. The final counter is a thin NaI(Tl) scintillator through which the protons pass, depositing an energy proportional to their dE/dx which decreases with increasing proton energy. For measurements of neutron spectra a polyethylene radiator is placed in front of the proton telescope to convert neutrons to recoil protons, and an anticoincidence counter is placed in front of the radiator to reject protons present in the incident flux.

The energy spectrum of incident protons or neutrons was calculated by using the pulse-height distribution from the dE/dx scintillator. The initial data analysis, under simplifying assumptions, related a given proton energy loss in the dE/dx scintillator to a corresponding proton or neutron energy. This method, however, ignored the finite energy resolution of the system. The resolution is governed primarily by the geometry of the spectrometer, the thickness of the radiator, if used, and the spread in energy deposited in the dE/dx detector due to the Landau effect. The composite resolution functions for neutrons and protons have been calculated, and the resulting pulse-height distributions are shown in Figs. 9.5.1 and 9.5.2 for various neutron and proton

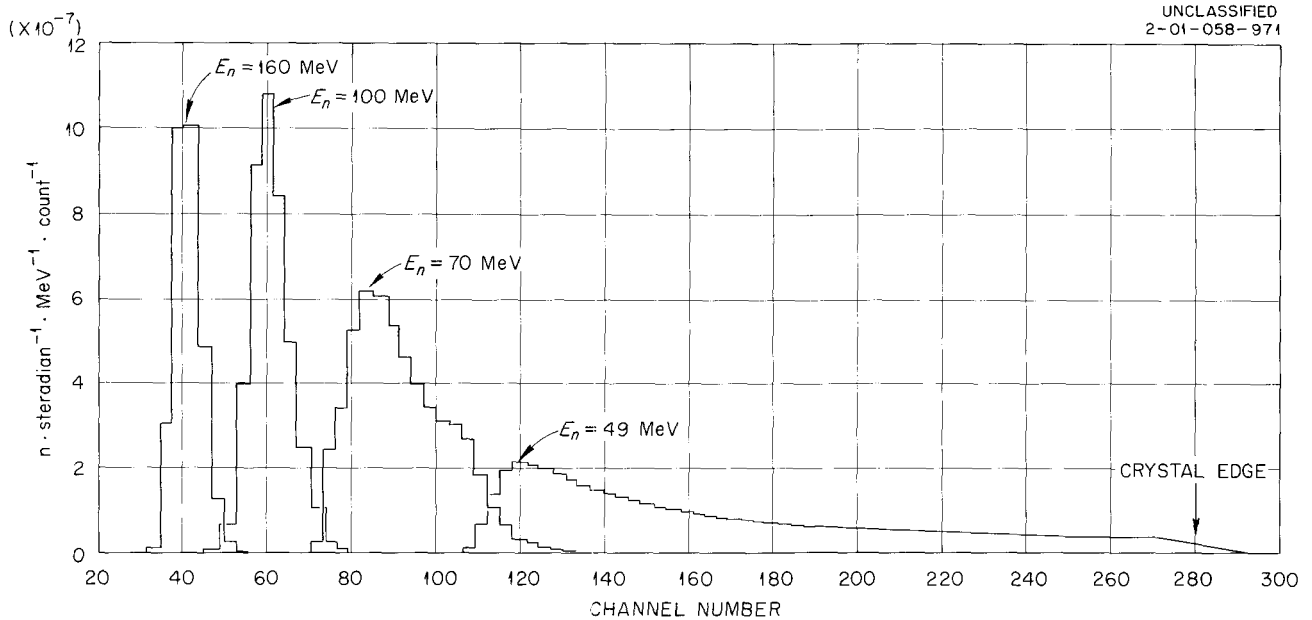


Fig. 9.5.1. Proton Spectrometer Response Functions for Various-Energy Neutrons. Radiator thickness: 1.334 cm.

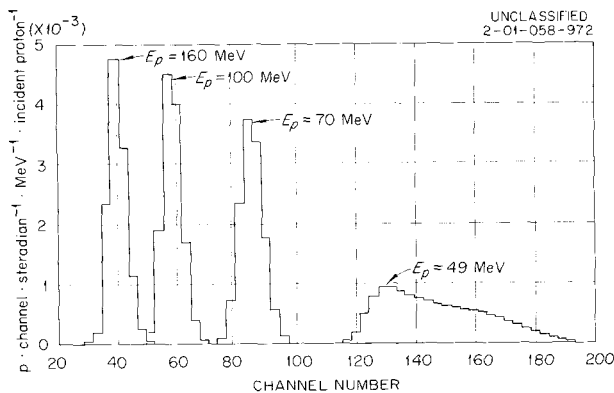


Fig. 9.5.2. Proton Response Matrix for Observations at 60° (Lab) with 30° Target Angle.

energies. These functions are somewhat skewed, and complicate comparisons of the results with other experimental results.

In order to present the results in a more standardized manner, the data are now being re-analyzed by using the SLOP code.² This code recombines the counting efficiency functions for each channel of the pulse-height distribution so that the resulting combinations approximate an idealized spectrometer having the desired re-

sponse function. The code is based upon "quadratic programming" and utilizes available *a priori* information in its operations. Thus the data were analyzed to make it appear that the spectra as presented had been measured with a spectrometer having Gaussian response functions of constant width. The advantages of such analyses are as follows:

1. The final spectrum is defined by two curves representing upper and lower limits of error at a given confidence level (usually taken as the 68% level) within which lies the true spectrum.

2. The final spectrum appears to have a Gaussian energy resolution, and may be compared statistically with a calculated spectrum by smoothing the calculated spectrum with a Gaussian of the same width.

3. The known nonnegativity of the spectrum and other information, such as the known regularity of the spectrum, are taken into account by the code. The use of this additional information results in a smaller uncertainty.

Typical results are shown in Figs. 9.5.3 and 9.5.4, Fig. 9.5.3 showing the spectrum for secondary neutrons from an aluminum target at 45° (laboratory system) and Fig. 9.5.4 giving the cross section for secondary protons from a bismuth

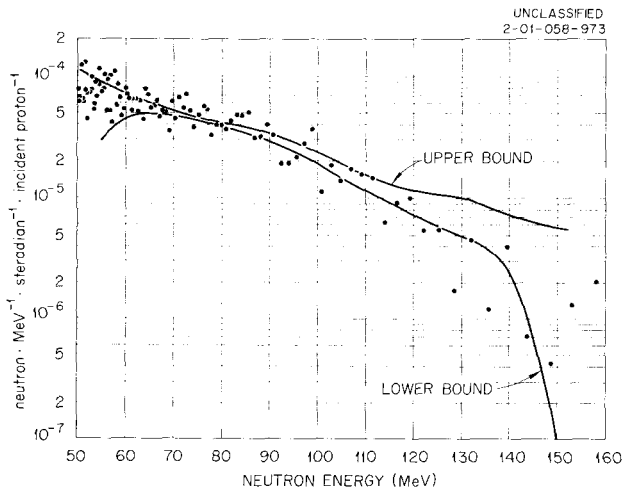


Fig. 9.5.3. Neutron Energy Spectrum for 160-Mev Protons Incident on a 26.9-g/cm²-thick Aluminum Target at 45° (Lab). Radiator thickness: 1.344 cm.

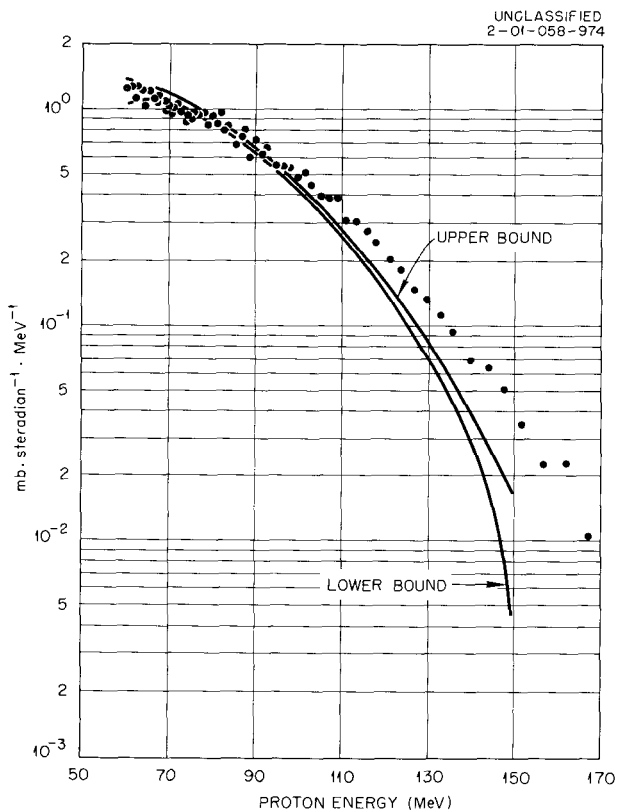


Fig. 9.5.4. Measured Proton Cross Section at 60° (Lab) for 160-Mev Protons Incident on a 0.866-g/cm²-thick Bismuth Target.

target at 60° (laboratory system). In both figures the measured data are shown as points; the curves indicate the derived limits of error at the 66% confidence level. The errors include the counting errors and the errors in smoothing the data to an apparent resolution of 25 Mev.

References

- ¹General Dynamics Corp., Fort Worth, Tex.
- ²W. R. Burrus, *Neutron Phys. Div. Ann. Progr. Rept. Aug. 1, 1963*, ORNL-3499, p. 120.

9.6. COMPARISON OF MEASURED NEUTRON AND PROTON SPECTRA WITH CALCULATED SPECTRA IN THE ENERGY REGION BETWEEN 50 AND 160 Mev

W. A. Gibson W. E. Kinney
W. R. Burrus J. W. Wachter
C. F. Johnson¹

The preceding section describes a measurement of the energy spectra of secondary neutrons and protons resulting from the bombardment of various targets by a collimated beam of 160-Mev protons. A principal objective of the experimental program of which these measurements are a part is to generate data to be compared with the Monte Carlo calculations of Bertini² and of Kinney.³

Two types of comparisons have been made for the energy region between 50 and 160 Mev. The first compared theoretical and measured cross sections for secondary neutron and proton production. The targets used in these experiments were thin, so that the incident proton lost less than 10% of its energy in traversing the target, and the probability of the secondary particles undergoing additional nuclear interactions was small. The second compared the measured neutron yield for targets sufficiently thick to completely stop the incident protons with the yield predicted by the Kinney transport code.

Two factors must be considered in making direct comparisons between the calculations and the measurements. First, the energy resolution

limitations of the spectrometer cause mixing of adjacent regions of the spectrum. This effect is especially significant when the energy spectrum changes rapidly, as in the case of proton cross sections. Second, the calculational model must correctly simulate the experimental conditions. For instance, angular data calculated without regard to the point of interaction are not comparable with experimental data, since for thick-target measurements a particle emitted at a given angle in the target may pass through the spectrometer, whereas a particle emitted at the same angle but at a point farther from the spectrometer may not enter it.

The effect of spectrometer resolution upon the data was considered by "smearing" the calculated spectrum with a Gaussian resolution function which closely approximated the resolution function used in analyzing the experimental results with the SLOP code.⁴ The correct calculational

model was obtained by writing a Monte Carlo analysis code which considered only those particles that corresponded to particles entering the spectrometer under actual experimental conditions.

Figures 9.6.1 and 9.6.2 show cross-section comparisons for protons at 60° and neutrons at 45° respectively. The hatched band in the figures is the 68% confidence interval obtained by the SLOP analysis of the data, while the errors shown for the calculated data are also 68% confidence limits. In both cases the errors are statistical only.

The theoretical and experimental cross sections, in general, agree at most points above 50 Mev. In a few cases agreement within the expected error is found for the total cross section over the entire energy range above 50 Mev. Three different potential well shapes were used, and the results giving the best overall agreement with experiment were chosen for these comparisons.

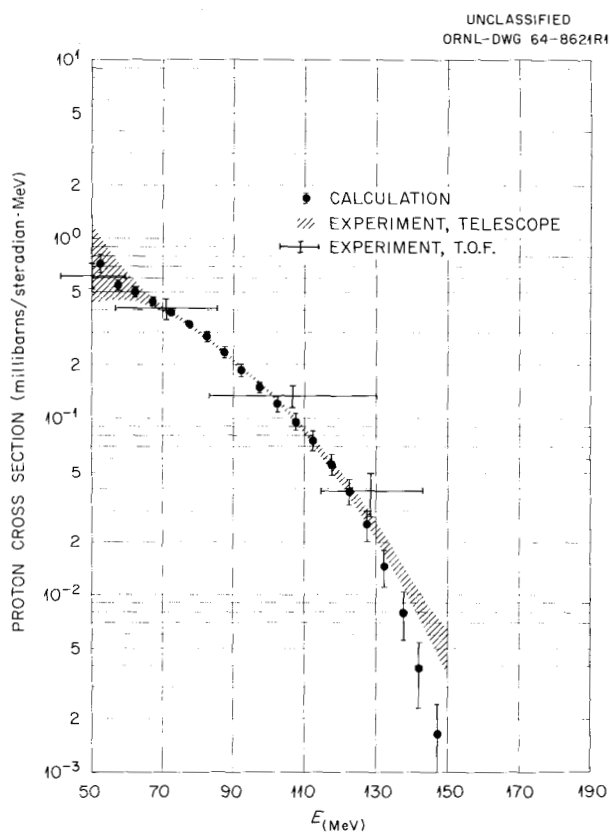


Fig. 9.6.1. Proton Production Cross Section at 60° as a Function of Energy for 160-Mev Protons Incident on a 0.549-g/cm²-thick Aluminum Target.

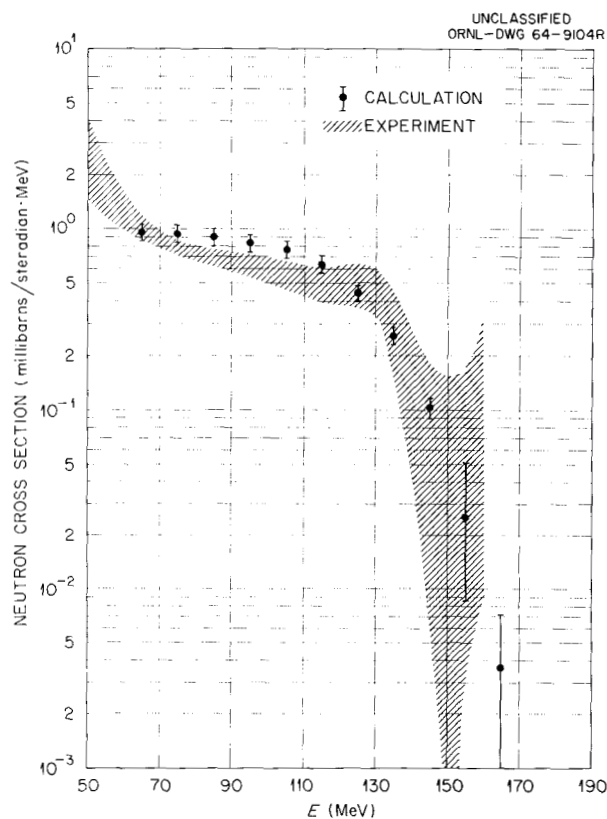


Fig. 9.6.2. Neutron Production Cross Section at 45° as a Function of Energy for 160-Mev Protons Incident on a 3.224-g/cm²-thick Cobalt Target.

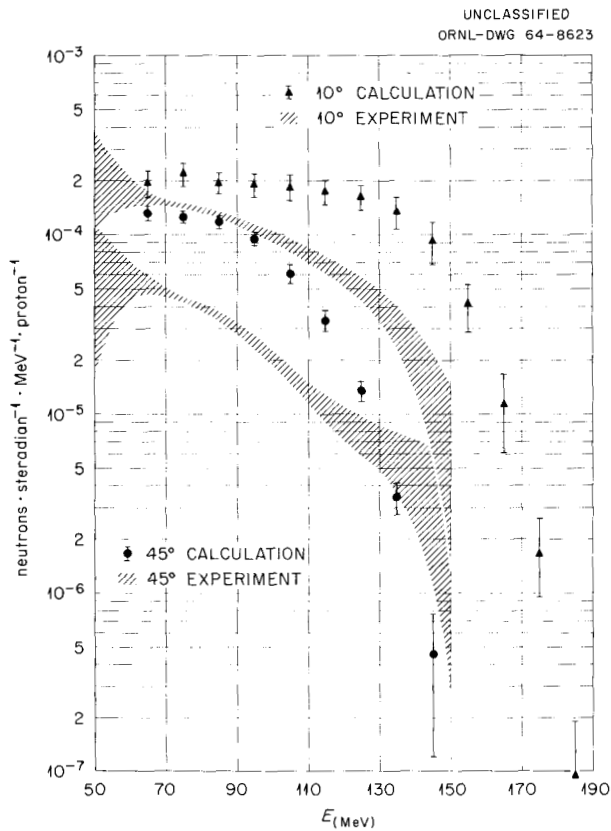


Fig. 9.6.3. Secondary Neutron Yield from a 26.89-g/cm²-thick Aluminum Target at 10 and 45° to the Incident 160-Mev Proton Beam. The incident beam was completely stopped in the target.

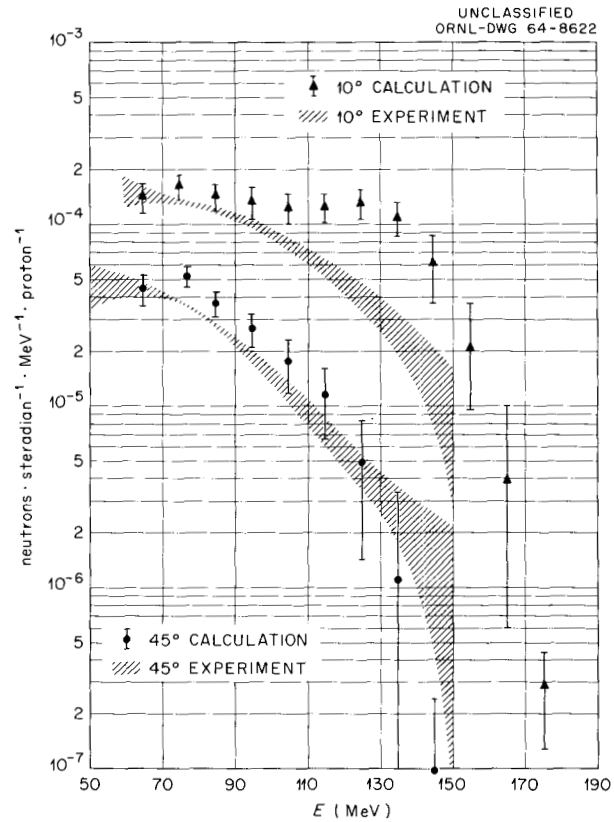


Fig. 9.6.4. Secondary Neutron Yield from a 44.33-g/cm²-thick Bismuth Target at 10 and 45° to the Incident 160-Mev Proton Beam. The incident beam was completely stopped in the target.

Figures 9.6.3 and 9.6.4 show theoretical and experimental neutron yields from 160-Mev protons on aluminum and bismuth respectively. Again the hatched band is the 68% confidence interval from the data analysis, and the errors shown for the calculated data are 68% confidence limits. A fairly serious disagreement appears to exist between the experimental results and those of the transport calculations, the calculated yields being larger in all cases. Little possibility exists for changes in the code, since the only variable parameters occur in the input data obtained from the cross-section code. Some effects, such as Coulomb scattering of the incident protons, have been included, and the inclusion of other factors which may improve agreement with experiment is being investigated.

References

- ¹General Dynamics Corp., Fort Worth, Tex.
- ²H. W. Bertini, *Monte Carlo Calculations on Intranuclear Cascades*, ORNL-3383 (April 1963).
- ³W. E. Kinney, *The Nucleon Transport Code, NTC*, ORNL-3610 (August 1964).
- ⁴W. R. Burrus, *Neutron Phys. Div. Ann. Progr. Rept. Aug. 1, 1963*, ORNL-3499, p. 120.

9.7. SPECTRA OF NEUTRONS AND PROTONS FROM TARGETS BOMBARDED BY 450-Mev PROTONS

W. A. Gibson W. R. Burrus J. W. Wachter

A measurement of neutron and proton spectra from targets bombarded by 450-Mev protons at

the University of Chicago Synchrocyclotron has been completed.¹ Although the data have not yet been completely analyzed, the details of the spectrometer and the types of data obtained may be summarized.

Basically the spectrometer is similar to the proton recoil spectrometer described previously,¹ with several modifications which improve its operation. As shown in Fig. 9.7.1, a hydrogenous radiator is preceded by two organic scintillation counters and followed by three organic scintillation counters and a Cerenkov detector. The two counters preceding the radiator are placed in anticoincidence with the other counters and serve to reject protons present in the incident flux. The three counters following the radiator are placed in coincidence, with the pulse height from the center counter being recorded in a pulse-height analyzer. The energy spectrum of the neutrons incident on the radiator is calculated from the pulse-height spectrum of the protons recoiling from the radiator. The other two coincidence counters limit the pulses being analyzed to those produced by charged particles (protons or electrons) passing completely through the region occupied by the radiator and the energy-detecting counter. The Cerenkov counter is placed in anticoincidence with the three counters, and

serves to reduce the background resulting from high-energy electrons produced by high-energy gamma-ray interactions in the target and radiator.

The major change from the previous spectrometer was the replacement of the NaI(Tl) energy detector with an organic scintillator whose light is collected from the side, thus permitting a counter to be placed behind the energy detector. Since the decay time of the light pulse from the organic scintillator is about 50 times faster than that of the pulse from NaI(Tl), a signal sufficient to trigger the coincidence circuit can be obtained with a much smaller average anode current in the photomultiplier. Since the maximum counting rate in the energy-detecting counter is governed by current-dependent gain shifts in the photomultiplier, the lower average anode current of the present spectrometer permitted an increase in the counting rate by a factor of 10.

The targets used in making the neutron measurements were carbon, aluminum, and cobalt. Target thicknesses were divided into two categories: those which absorbed less than 60 Mev from the incident proton beam, and those which absorbed more than 200 Mev. Small-angle measurements were also made with a cobalt target which completely stopped the incident protons, but physical limitations on the thickness of the targets pre-

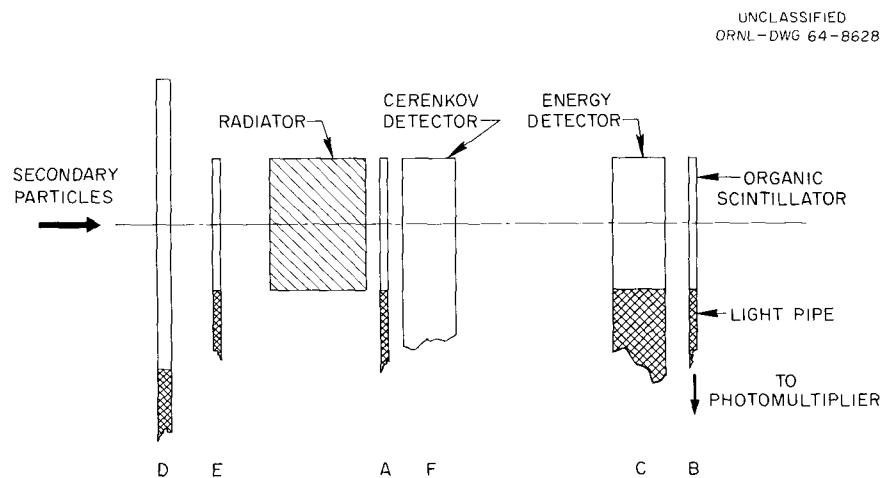


Fig. 9.7.1. Diagram of Proton Recoil Spectrometer Used To Measure the Spectra of Secondary Neutrons and Protons from Targets Bombarded by 450-Mev Protons. The organic scintillators A, B, and C are placed in coincidence and detect the protons recoiling from the radiator. Scintillators D and E are in anticoincidence with ABC to reject counts due to protons in the incident beam. A Cerenkov counter, F, in anticoincidence with ABC, serves to reject counts due to electrons resulting from interaction of gamma rays with the targets and radiator.

vented such measurements with the less dense elements. The angular region covered was from 0 to 45°.

A wide variety of elements, with atomic weights ranging from 9 to 209, were used as targets for the proton measurements. All targets absorbed less than 10 Mev from the incident beam. The angular interval covered was from 30 to 120°.

The data are being analyzed by methods described previously,² and will be compared with results of cross-section³ and transport calculations.⁴

References

¹W. A. Gibson *et al.*, *Neutron Phys. Div. Ann. Progr. Rept. Aug. 1, 1963*, ORNL-3499, Vol. II, p. 109.

²J. W. Wachter *et al.*, *Neutron Phys. Div. Ann. Progr. Rept. Aug. 1, 1963*, ORNL-3499, Vol. II, p. 89.

³H. W. Bertini, *Monte Carlo Calculations on Intranuclear Cascades*, ORNL-3383 (Apr. 23, 1963).

⁴W. E. Kinney, *The Nucleon Transport Code, NTC*, ORNL-3610 (August 1964).

9.8. MEASUREMENTS OF PROTON-INDUCED GAMMA-RAY SPECTRA AT ORIC

W. Zobel R. T. Santoro
J. H. Todd¹ F. C. Maienschein

Measurements of the energy spectra of gamma rays produced in six target materials by 160-Mev incident protons, which are required for calculations of the gamma-ray doses that will be received by astronauts during space flight, were discussed in Sect. 9.3. Because of the variety of proton-induced reactions and the uncertainties in their energy dependencies, spectral measurements are also required at lower proton energies in order to make reasonably accurate dose calculations. Both the proton intensity in solar flares and the interaction cross sections increase at lower energies. Equipment for such measurements has been set up at the Oak Ridge Isochronous Cyclotron (ORIC). The two gamma-ray spectrometers are basically the same as

those used for the 160-Mev measurements – a three-channel “pair” spectrometer and a total-absorption spectrometer. Major problems to be overcome include rejection of the neutron background and control of count losses, which tend to be large because of the pulsed nature of the cyclotron beam and because of the high singles counting rates that are required in order to obtain useful statistics from the low-efficiency coincidence spectrometer.

The standard ORIC ion optic system, consisting of a single quadrupole lens and a four-jaw collimator, in addition to a common steering magnet, is used to direct the proton beam to a target mounted in a helium-filled chamber. Focusing is achieved by optimizing the quadrupole magnet current and collimator jaw openings. The target thickness is nominally 15% of the total proton energy, permitting continuous absolute-beam-intensity measurements with a Faraday cup. The target is viewed by the spectrometer, which is constrained to rotate about the proton beam axis through an angle of 140° at a distance of 1 m. The beam position is determined by occasional exposure of Polaroid film. The beam energy is determined by a measurement of the range in aluminum of protons which are scattered from a thin (~3-mil-thick) hydrogenous foil. Measurements of the first proton energy chosen for use gave a value of 34.4 ± 1.0 Mev.

The variation in time of the cyclotron beam should, in principle, be limited to microstructure at the frequency used (57.5-nsec separation between bursts at the energy given above). In common with all cyclotrons, however, additional time structure exists in the ORIC beam at several lower frequencies, which reduces the effective beam duty factor. Nonexhaustive studies of the effect on the additional structure of changes in cyclotron parameters led to the conclusion that they could not be eliminated by parameter variations within the design limits. Since the duty factor is not constant with time, the count losses must be measured continuously.

For the three-channel pair spectrometer, the coincidence timing signals are obtained from a crossover pick-off circuit which senses the return of the voltage pulse to the base line. Pileup of pulses leads to a change in shape and thus in the pick-off time, so that timing signals are removed from coincidence and counts are lost. A system has been devised which measures

this loss during a spectrum measurement. It consists essentially in determining the loss in an added channel caused by introducing a signal from a second channel for which the gain is adjusted to maintain the proper relationship in magnitude between the two signals. The rapid variations in counting rate with cyclotron output are reflected in the count-loss measurement. In practice, the gain adjustment and the detailed analysis of the measurements are difficult. In one measurement with a 0.49-g/cm²-thick aluminum target at 34 Mev, a 10% overall counting loss was observed for a pair-coincidence-counting rate of 20 counts/sec. The no-target background was ~2 counts/sec. The cyclotron duty factor for this run was of the order of 30%.

The major loss of counts for the total-absorption spectrometer occurs in the pulse-height analyzer, where it is accurately determined by the ratio of the analyzer "live" time to "real" or clock time. For the same beam strength used for the pair measurement, the analyzer loss was about 20%.

In the use of scintillation spectrometers to determine energy spectra, attention must be given to gain shifts in the photomultiplier tubes when high counting rates are encountered. In order to control the gain shifts, it was necessary to select photomultipliers having small gain shifts. Wide variations were observed during the selection. The high-gain 56 AVP chosen for the center channel of the spectrometer exhibited a gain shift of 1.3% for a change in average anode current from 50 to 1000 μ a, corresponding to a maximum count rate of ~50,000 counts/sec due to a ¹³⁷Cs source. The overall photomultiplier voltage was 1920 v. The other photomultipliers, of type 6363, gave gain shifts of <0.5% for count rates from 600 to 20,000 counts/sec at 511 kev with a tube voltage of 650 v.

The energy calibration of the spectrometer is obtained by exposing it to radioactive sources having energies up to 2.75 Mev (with useful half-lives). Those sources which have suitable decay schemes may also be used for efficiency calibrations. The absolute disintegration rates of such sources have been determined by use of the calibrated high-pressure ionization chamber.² A calibration source for energies above 3 Mev is necessary but difficult to obtain; however, it is planned to use the ¹¹B(p, γ)¹²C reaction which yields 4.4- and 11.8-Mev gamma rays.

Finally, it is necessary to consider the neutron-induced background in the gamma-ray spectral measurements. Lead absorption measurements with the 0.49-g/cm²-thick aluminum target at 34 Mev indicated a neutron background of 15% for both spectrometers. In the earlier 160-Mev measurements the background was larger; it was ~45% for an aluminum target and was only reduced to 20% by using time-of-flight techniques to discriminate against neutron-induced events. The time zero was derived from a scintillator placed in the proton beam. As a simplification, it was attempted at ORIC to use a timing signal derived from the cyclotron rf as the time reference. This method works well, and time variations between signals derived from the two methods are less than 1.5 nsec. However, additional measurements have demonstrated that the walk of the signal used for timing the spectrometer pulse is greater than was realized at the time of the 160-Mev measurements; this walk must be reduced to maintain fast timing (~5 nsec resolving time) and thus make the time-of-flight rejection system worthwhile.

In the results obtained at 160 Mev, many assignments of peaks in the gamma-ray spectra were uncertain because the energy resolution of the scintillation spectrometer was inadequate to separate levels in mirror nuclei or accidentally nearly coincident levels. The much improved energy resolution of the lithium-drifted germanium solid-state spectrometer³ is therefore highly attractive, and a 4-mm-thick diode has been obtained. Problems associated with its requisite operation at liquid-nitrogen temperature and its lower efficiency are being investigated. It is not yet clear whether this spectrometer will supplement or replace the scintillation spectrometer.

References

- ¹Instrumentation and Controls Division.
- ²R. W. Peelle, *Use of 4 π High-Pressure Ionization Chambers as Secondary Standards for Calibration of Gamma-Ray Sources*, ORNL-CF-61-4-32 (Apr. 17, 1961).
- ³G. T. Ewan, *The Use of Germanium Lithium-Drifted p-i-n Diodes as High-Resolution Gamma-Ray Spectrometers*, AECL-1960 (April 1964).

9.9. THE ENERGY DEPOSITION IN A WATER-FILLED SPHERICAL PHANTOM BY SECONDARIES FROM HIGH-ENERGY PROTONS AND BY NEUTRONS¹

T. V. Blosser F. C. Maienschein
R. M. Freestone, Jr.

The energy deposited by neutrons, gamma rays, high-energy protons, and the nuclear secondaries resulting from the interaction of high-energy protons with several targets has been measured at various points within a 42-cm-diam spherical water-filled Lucite phantom. The proton source was the Harvard University Synchrocyclotron, producing protons of nominally 160-Mev energy. Targets were H₂O, Al, C, Cu, and Bi. For neutrons the ³H(d,n)⁴He reaction, giving ~14.9-Mev neutrons, and a Po-Be source ($\bar{E}_n = 4.3$ Mev) were used. The gamma-ray source was ⁶⁰Co. The detectors were small Lucite-walled ionization chambers filled with either ethylene or 97% Ar - 3% CO₂ gas.

Data were taken at the cyclotron both with the phantom on the beam axis and with the phantom offset ~55° from the beam axis. The proton beam energy determined from a part of these results, ~160 Mev, is in good agreement with published values. The energy deposited by secondary particles was found to increase with the atomic number of the target material, as expected. The depth-dose curves have a steeply negative slope over the region near the surface of the phantom, and a more gentle slope at greater depths. The magnitude of the dose in the region of the initial slope decreases with increasing target thickness, while at greater depths it increases. The dose in the region of initial slope is presumably due to secondary protons, while at greater depths it is principally controlled by secondary-neutron interactions.

With an aluminum target thicker than the incident proton range, the absorbed dose at ~55° from the beam axis was only about 20% of that at 0°. Comparison of the slopes of the curves of depth dose due to the secondaries (assumed to be largely neutrons) from this target with the slopes of the curves for neutron sources suggests that the effective energy of the secondaries is greater than 15 Mev.

These experimental data will permit detailed comparisons with calculations of the physical

dose due to secondaries from high-energy protons. The results of such calculations are not yet available.

References

¹Abstract of published paper: *Health Phys.* **10**, 743 (1964).

9.10. RESULTS FROM NUCLEAR EMULSIONS EMBEDDED IN A STEEL SHIELD EXPOSED TO A 10-GeV/c PROTON BEAM

R. L. Childers¹ C. M. Fisher³
C. D. Zerby² R. H. Thomas³

The work reported here is a continuation of previously reported studies⁴ of nuclear showers induced in various shielding materials by highly energetic protons of energies ranging from 9 to 30 Gev. In the present experiment, nuclear emulsions were placed at various positions in a steel shield exposed to a 10-GeV/c proton beam. The exposed emulsions were scanned for shower track intensity, defined as the number of charged particles above a certain energy crossing the unit area per incident beam particle, and for star density, defined as the number of nuclear interactions per unit volume.

The present results were expected, and confirm earlier work in which concrete was used as the shielding material. The minimum ionizing peak track density is attenuated with a mean free path of 119 g/cm², and after a transition region of ~3λ the integrated minimum track intensity decreases roughly exponentially, with a somewhat longer attenuation length. The present work indicates that the muon tail seen in some of the earlier work was probably due to inadequate background correction.

The measured charged-star density along the beam axis is closely related to the track density. There is some evidence that the incident proton beam was surrounded by a halo of collimator-scattered particles. The fraction of neutral stars in the forward portion of the shield indicates a 25% contamination of neutrons having energies around 1 Gev. Furthermore, the "shoulder" observed in the track density profiles could well be interpreted as due to pions and electrons

produced in the collimator. This suggestion is further supported by the absence of such a shoulder in charged-star lateral profiles. The proportion of neutral stars increases toward 100% as the mean energy of the charged component diminishes. At about 500 Mev the range of a proton is equal to its reaction mean free path, and so at energies much below 500 Mev the probability of a proton reaction before the proton is stopped is quite small. This region is reached at a depth of 200 cm in steel for 10-Gev/c incident protons.

References

¹Present address: University of South Carolina, Columbia.

²Union Carbide Research Institute, Tarrytown, N.Y.

³Rutherford Laboratory, N.I.R.N.S., England.

⁴R. L. Childers, *Neutron Phys. Div. Ann. Progr. Rept. Sept. 1, 1962*, ORNL-3360, p. 241; see also *Neutron Phys. Div. Ann. Progr. Rept. Aug. 1, 1963*, ORNL-3499, Vol. II, p. 14. A complete account of all portions of this work is to be published in *Nuclear Instruments and Methods*.

9.11. DIFFERENTIAL AND TOTAL CROSS SECTIONS FOR THE ${}^9\text{Be}(\alpha, n)$ REACTIONS FROM 6 TO ~ 10 Mev¹

V. V. Verbinski	J. Gibbons ²
W. R. Burrus	W. E. Kinney
J. K. Dickens	R. L. Macklin ²
F. G. Perey	

Measurements of total and differential cross sections for the ${}^9\text{Be}(\alpha, n)$ reaction have been made for alpha-particle energies up to 10 Mev. The beam of α^{2+} particles was obtained from the ORNL 5.5-Mev Van de Graaff accelerator. The total cross sections were measured with the ORNL graphite-sphere long counter, but because the sphere efficiency drops off above 8 Mev, the neutron spectral intensities were obtained with a 2- by 2-in.-diam NE-213 liquid scintillator³ spectrometer having a low-energy bias of 0.5 Mev. The differential data for energies above 8 Mev were then employed to

correct the total cross-section data for the "nonflat" response of the long counter.

Angular and spectral measurements, in addition to being useful to the measurement of total cross sections, are of significant interest to the study of nuclear reaction mechanisms. This is especially true when the incident particle is an alpha particle, for which calculations and interpretation of experimental results are simplified by virtue of the alpha particle being a tightly bound spin-zero particle.

Figure 9.11.1 shows the total ${}^9\text{Be}(\alpha, n)$ cross section and the 0° (c.m.) excitation functions (in mb/steradian) for the n_0 , n_1 , and n_2 neutron groups from the ${}^9\text{Be}(\alpha, n){}^{12}\text{C}$, ${}^{12}\text{C}^*$ reactions, leaving ${}^{12}\text{C}$ in the ground, first, and second excited states respectively. Both the total and the differential cross sections show a significant amount of structure, which is characteristic of compound nucleus effects. Because of this structure, the falloff of σ_T above 9.1 Mev is likely to be local and may not continue to decrease above 10.5 Mev. In other measurements⁴ of n_0 and n_1 neutron angular distributions from ${}^9\text{Be}(\alpha, n){}^{12}\text{C}$, ${}^{12}\text{C}^*$ reactions, the structure was observed to vanish above 17 Mev (a strong forward peaking sets in, indicative of direct interaction); therefore the total cross section above 17 Mev should be smoother and more reliably extrapolated. Measurements above 17 Mev should be made since the ${}^9\text{Be}(\alpha, n)$ cross section is of particular concern to spacecraft designers considering beryllium alloys because of the alpha particles in solar flares.

In obtaining the differential data a pulse-shape discrimination⁵ was used to reject gamma-ray counts. A few samples of the spectra unfolded with the SLOP code (see Sect. 6.1) are shown in Fig. 9.11.2. The data for a 10.1-Mev alpha bombarding energy yield four distinct peaks: n_0 , n_1 , n_2 , and n_3 neutrons from the ${}^9\text{Be}(\alpha, n){}^{12}\text{C}$, ${}^{12}\text{C}^*$ reactions.

Analysis of the data was delayed because the scintillator response to monoenergetic neutrons, which is a required input to the SLOP unfolding code, was accurately calculable to only 11 Mev (see Sect. 6.2). However, Monte Carlo calculations of the response functions for organic scintillators have been modified to include $(n, n', 3\alpha)$, (n, α) , (n, p) , and (n, pn) reactions on the ${}^{12}\text{C}$ of the scintillator, and reliable calculations of scintillator response were made possible for energies up to 25–30 Mev. These have satisfactorily re-

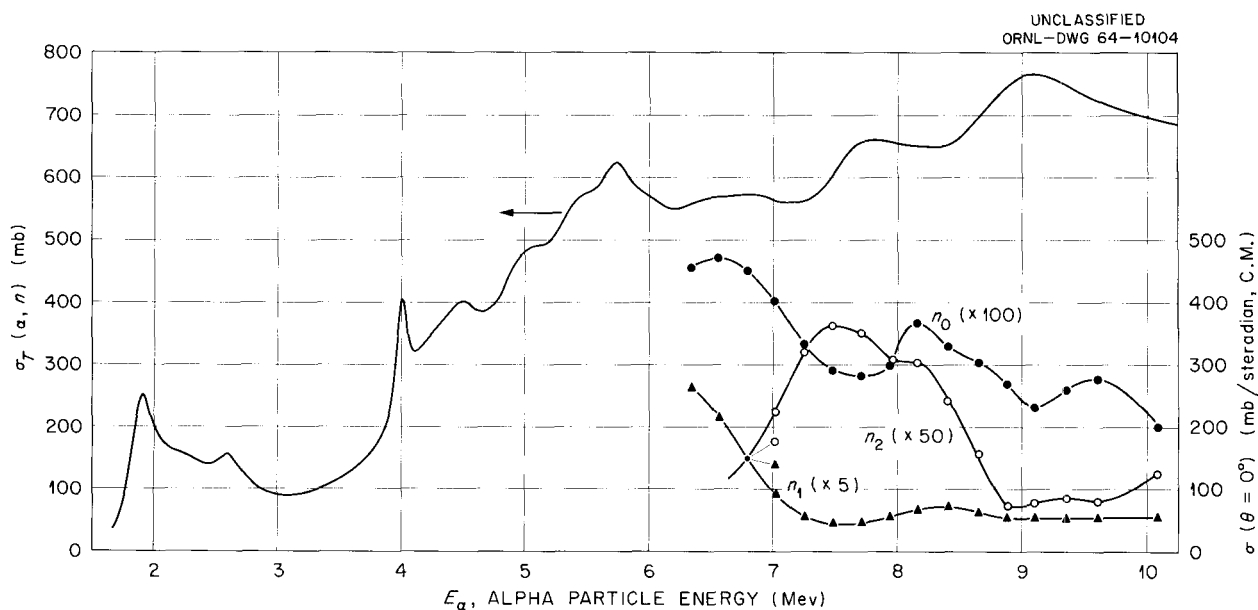


Fig. 9.11.1. Total Neutron Yield from ${}^9\text{Be}(\alpha, n)$ Reactions and 0° Excitation Functions for n_0 , n_1 , and n_2 Neutrons.

produced the pulse-height distribution obtained for 14.4-Mev incident neutrons with an NE-213 scintillator.

The scintillator resolution has recently been improved by a factor of about 2 by substituting an aluminum-foil reflector for the manufacturer's white paint reflector on a 2- by 2-in.-diam NE-213 glass-encapsulated scintillator. With this, it is hoped that we can resolve n_0 , n_1 , n_2 , and n_3 neutrons from the ${}^9\text{Be}(\alpha, n){}^{12}\text{C}$, ${}^{12}\text{C}^*$ reactions for alpha bombarding energies above 20 Mev and can use the relatively weak beam from the ORNL tandem Van de Graaff.

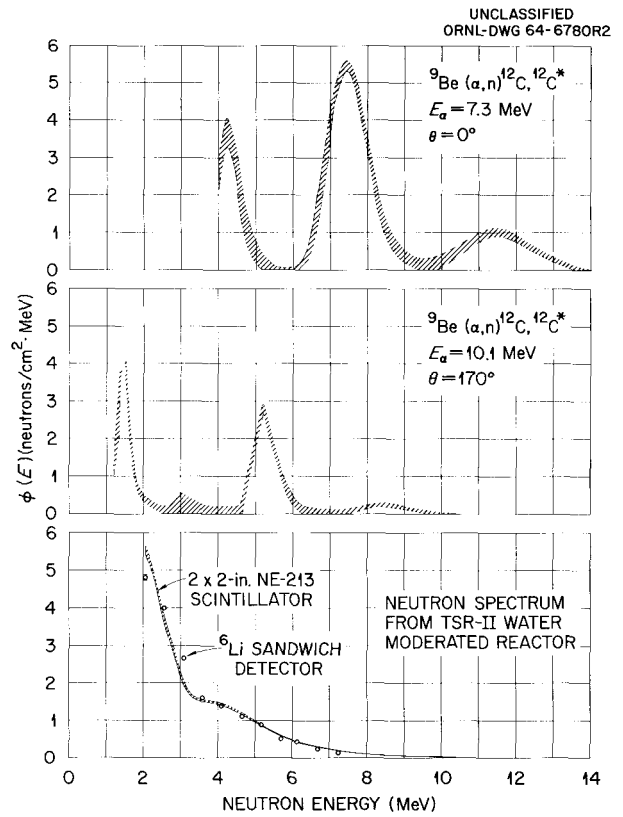
The n_0 and n_1 neutron angular distributions have been obtained with hand calculations at 7.3-, 8.2-, 9.2-, and 10.1-Mev alpha bombarding energies. In general, their structure (shape) is pronounced, with two to three maxima, and varies slowly with energy; an exception is the rather large change for the n_0 angular distribution between 7.3- and 8.2-Mev alpha energies. At 10.1 Mev, the angular distributions are in good overall agreement with the 9.8-Mev results of Kjillman and Nilsson⁶ for n_0 and n_1 neutrons.

The work reported here represents an extension of total cross-section measurements performed previously by Gibbons and Macklin.⁷

References

- ¹Same as Sect. 1.17 in Vol. I; repeated here because of its significance to the NASA Space Shielding Program.
- ²Physics Division.
- ³Nuclear Enterprises, Ltd., Winnipeg, Manitoba, Canada.
- ⁴G. Deconnick *et al.*, *Nucl. Phys.* **49**, 424 (1963).
- ⁵V. V. Verbinski *et al.*, *Neutron Phys. Div. Ann. Progr. Rept. Sept. 1, 1962*, ORNL-3360, Fig. 6.17.2, p. 107.
- ⁶J. Kjillman and A. Nilsson, *Arkiv Fysik* **22**, 277 (1962); A. Nilsson and J. Kjillman, *Nucl. Phys.* **32**, 177 (1962).
- ⁷J. H. Gibbons and R. L. Macklin, *Phys. Rev.* **114**, 571 (1959); R. L. Macklin, *Nucl. Phys.* **1**, 335 (1963).

Fig. 9.11.2. Sample Energy Spectra Obtained from Unfolding Pulse-Height Distributions from the ${}^9\text{Be}(\alpha, n)$ Reactions. Up to four neutron groups are identified from the ${}^9\text{Be}(\alpha, n){}^{12}\text{C}, {}^{12}\text{C}^*$ Reactions.



10. Radiation Detector Studies (II)

10.1. MEASUREMENT OF THE ABSOLUTE EFFICIENCY OF NE-213 ORGANIC PHOSPHORS FOR THE DETECTION OF 14.4- AND 2.6-Mev NEUTRONS

T. A. Love R. W. Peelle
R. T. Santoro N. W. Hill¹
R. J. Schuttler²

The absolute efficiencies of two 12-cm-diam NE-213 scintillators,³ one 2.54 cm thick and the other 6.10 cm thick, were determined experimentally for neutrons having energies of 14.4 ± 0.3 and 2.6 ± 0.1 Mev. The associated particle technique,⁴ utilizing the recoil particles from the ${}^3\text{H}(d,n){}^4\text{He}$ ($E_d = 135 \pm 5$ kev) and $\text{D}(d,n){}^3\text{He}$ ($E_d = 85 \pm 5$ kev) reactions, was employed. In these reactions each neutron has associated with it a helium particle which is emitted at an angle of 180° with respect to the neutron in the center-of-mass system. If the deuteron energy is known and the helium particles are detected within a well-defined laboratory solid angle, then the energy, angle of emission, number, and timing of the conjugate neutrons are given. If the number of helium particles is known, the efficiency of a neutron detector placed in coincidence with the particle detector is obtained from the ratio

$$\epsilon = \frac{\text{neutron-helium particle coincidence counts}}{\text{total number of helium particle counts}}$$

Appropriate care must be taken to discriminate between the various recoil particles, since deuterium buildup in the tritium targets results in the emission of protons by the competing $\text{D}(d,p){}^3\text{H}$ reaction.

Figure 10.1.1 is a block diagram of the apparatus used in the experiment. The deuteron beam was produced by a small, positive-ion accelerator.

A housing located at the end of the beam pipe contained the beam collimator, the target, the absorber foils, and the charged-particle detector. The thick targets consisted of $500 \mu\text{g}/\text{cm}^2$ of titanium evaporated on 20-mil-thick plates, the titanium being saturated with tritium or deuterium.⁵

The charged-particle detector was a silicon surface-barrier diode⁶ which had a 50-mm^2 sensitive area and was fixed at 120° with respect to the beam. A bias voltage of 100 v, which fully depleted the $200\text{-}\mu$ 3200 ohm-cm detector, was used. The overall resolution of the detector for charged particles was 100 kev, giving very nearly 100% detection efficiency. In order to ensure that only the proper charged particles were counted, a "window" was set across the pulse-height distribution peaks of the ${}^3\text{He}$ or ${}^4\text{He}$ particles. The apparent efficiency was observed as a function of window width and position, and for the final measurements the window was set within the range which gave constant efficiency.

The NE-213 scintillators, mounted on type 58 AVP photomultiplier tubes, could be varied in position with respect to the beam, thus ensuring that every neutron associated with a detected charged particle entered the flat face of the scintillator. On the face of each neutron detector was also mounted a thin NE-102 detector³ (identified as C in Fig. 10.1.1). This detector, although not required for these measurements, formed part of the configuration for which the efficiency was desired. It had been used in an earlier experiment with a coincidence device to discriminate between charged particles and neutrons, both incident on the NE-213 detectors.

A charged particle incident upon the solid-state detector produced a pulse that was amplified, split, and fed through two discriminators which established the upper and lower limits of the

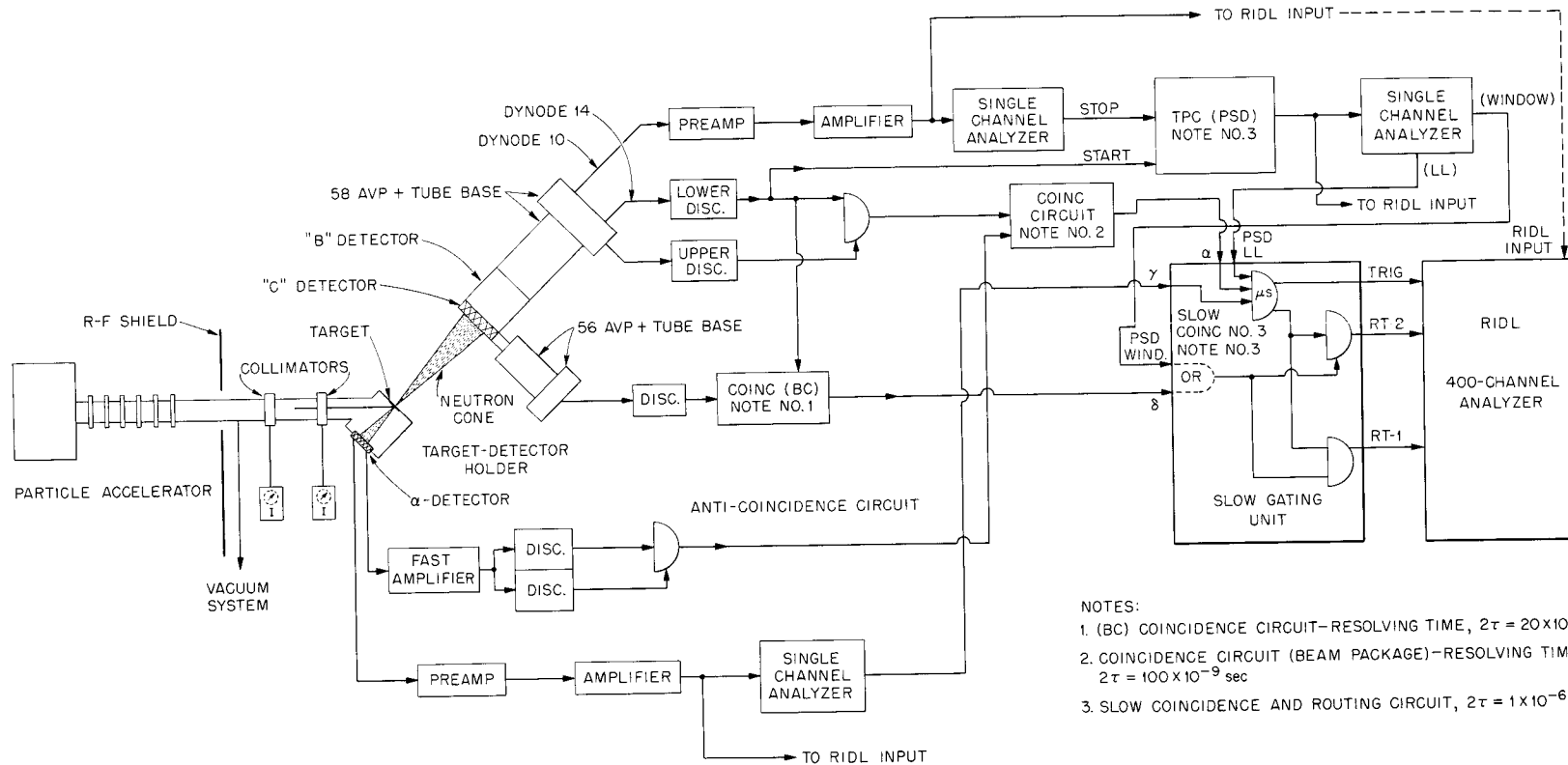


Fig. 10.1.1. Block Diagram of Experimental Arrangement and Electronic Circuitry for Measurement of Scintillator Efficiency.

window across the ^3He or ^4He pulse-height distribution peaks. The pulses produced by neutrons followed a similar path and were placed in coincidence with the charged-particle pulses. Together, the coincidence counts and the corresponding singles counts from the charged-particle detector gave the information needed to calculate the efficiency from the ratio given above. Additional outputs from each detector were fed through slow electronic systems for a multichannel analysis of the pulse-height spectra.

Pulse-shape discrimination was used to distinguish between heavy charged particles and gamma rays in the NE-213 scintillator by observing the variation in time of the zero crossover point of bipolar pulses from a standard double-delay-line amplifier. Measurements were made to estimate the fraction of pulses due to neutrons which were mistaken for gamma-ray pulses.

The controlling bias of the neutron detector, measured with electron total light, was determined with the gamma rays from ^{60}Co , ^{113}Sn , Po-Be, and ThC". The pulses accepted as proton recoils were those with a fast component equal to or greater than that produced by the Compton electrons of the appropriate energy.

The efficiency of each of the two detectors studied is plotted in Fig. 10.1.2 as a function of the bias applied to the detector. Where experimental errors are not shown, the error is within the size of the point. Agreement with the values computed by Verbinski *et al.* (Sect. 6.2) is within 5 to 7%. Values obtained for the efficiency in the energy range below 1 Mev (electron light) are 20% larger than those previously calculated (Sect. 10.14); however, the calculations did not include the effects of the $^{12}\text{C}(n,\alpha)^9\text{Be}$ reaction nor the contribution due to neutrons which initially passed through the detector but were backscattered into it by the light pipes.

References

- ¹Instrumentation and Controls Division.
- ²Centre D'Etudes Nucleaires, Fontenay-aux-Roses, France.
- ³Nuclear Enterprises, Ltd., Winnipeg, Canada.
- ⁴F. G. J. Perey, *Inelastic Scattering of 14-Mev Neutrons in Carbon, Oxygen, and Lithium*, Thesis, University of Montreal, Canada (1960).
- ⁵Obtained from the Isotopes Division.

⁶Oak Ridge Technical Enterprises Corp., Oak Ridge, Tenn. It was mounted in the detector-target housing by R. E. Zedler, Instrumentation and Controls Division.

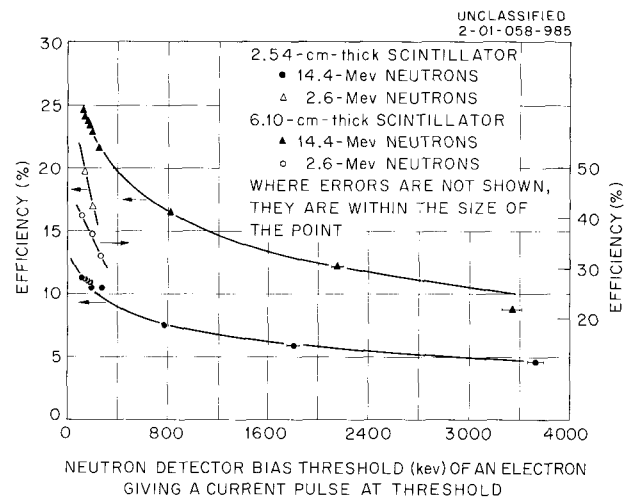


Fig. 10.1.2. Scintillator Efficiency as a Function of Detector Bias Threshold.

10.2. MEASUREMENTS OF THE FAST AND TOTAL LIGHT RESPONSE OF NE-213 SCINTILLATORS TO CHARGED PARTICLES

T. A. Love R. J. Schuttler¹

The rapidly increasing use of solid and liquid organic phosphors for the study of neutron spectra makes it necessary that the light output of such phosphors be better understood. By a careful analysis of pulse shapes resulting from the light output, pulses due to electrons can be identified separately from those due to heavy particles such as protons and alpha particles, and several investigators²⁻⁵ have reported methods and circuits for doing this. In the experiments described here the fast and total light output from alpha-particle and proton-induced scintillations were measured relative to that induced by electrons in NE-213,⁶ a deoxygenated liquid scintillator.

Two NE-213 scintillators, 1.5 in. in diameter and 1.5 in. high and contained in aluminum cans with glass faces, were used for the measurements with

alpha particles. A 4.76-Mev alpha source (^{234}U) was evaporated on a platinum disk and glued to the side of one of the cans near its top, while a similar 6.10-Mev source (^{242}Cm) was glued to the side of the other can. Both sources had areas of about 0.8 cm^2 .

Gamma-ray sources (^{113}Sn and ^{137}Cs) were used to calibrate bias settings and to adjust the gain. Current pulses from dynode 14 of a 56 AVP photomultiplier tube were fed into a tunnel diode discriminator, which therefore responded at threshold only to the fast portion of a pulse. The threshold level was controlled by adjustment of the bias current through the tunnel diodes. Pulses time-integrated over $0.7\text{ }\mu\text{sec}$ were fed to a multi-channel analyzer only if the current pulse fired the fast discriminator (see Sect. 10.8). Thus the low pulse-height cutoff represents the total amount of light for a given amount of fast light. Calibration was made in terms of the total light induced by the Compton electron from gamma rays of known energy. The relative equivalent of fast light for the alpha sources was found by plotting a curve of counts per unit time vs an integral bias level.

The results of the measurements with alpha particle sources are shown in Table 10.2.1. The gamma rays used for calibration uniformly illuminated the detector from a distance of about 50 cm. However, comparison of the gamma-ray pulse height produced by gamma rays collimated into the detector perpendicularly to its axis at a point near the alpha source with the pulse height for uniformly illuminating gamma rays showed a difference in gain of about 15%. A correction for this difference has been made.

A major source of uncertainty in the measurements and their analysis was the apparent difference in gain, in terms of kev per channel, in the total light pulse-height spectra from ^{113}Sn and ^{137}Cs , the latter giving about 7.5% greater gain than the former. The calibration of the ^{234}U source was therefore based solely upon the total light induced by the ^{113}Sn source, while for the ^{242}Cm source the calibration was based upon the average gain of the two gamma-ray sources.

For the measurements of the proton-induced fast and total light output, a window, operating only on the fast portion of the pulse (see Sect. 10.1), was set at several points on the pulse-height distribution curve observed for 14.4-Mev neutrons incident on a 5-in.-diam by 1-in.-high NE-213 scintillator mounted on a 58 AVP photomultiplier tube. Pulses time-integrated over $0.7\text{ }\mu\text{sec}$, which included most of the light, were stored in a multichannel analyzer. Total-light pulses from incident gamma rays were similarly stored. The ratio of the mid-window channel number for protons to that for electrons is shown in Table 10.2.2.

Table 10.2.1. Comparison of the Energies of Alpha Particles and Electrons Producing Equivalent Fast and Total Light

Alpha-Particle Energy (Mev)	Electron Energy (kev)	
	For Equivalent Fast Light	For Equivalent Total Light
4.765 ± 0.003	214 ± 10	300 ± 15
6.110 ± 0.005	338 ± 15	540 ± 25

Table 10.2.2. Ratio of the Total Light Output of Protons to That of Electrons for a Given Fast Component

Electron Energy Producing Fast Component (Mev)	Gamma-Ray Source	Mid-Window Channel Number		Ratio of Proton Channel to Electron Channel
		Proton	Electron	
0.229 ± 0.010	^{60}Co	62.5	41	1.52
0.239 ± 0.010	^{60}Co	31	22	1.40
0.831 ± 0.030	^{60}Co	100	78	1.28
1.96 ± 0.2	ThC	112	100	1.12
3.74 ± 0.112	Po-Be	72	68	1.06

The fast light output of an organic scintillator was assumed to be given by the integral of the equation⁷

$$\frac{dF}{dE} = \left(1 + B \frac{dE}{dX}\right)^{-1}, \quad (1)$$

where dE/dX is taken as a positive quantity, E is the energy of the incident particle, and F is the energy of an electron which would give the same amount of fast light. Equation (1) is not exactly valid for electrons, but the assumption permits a calculation of B from our data.

A method due to Peelle (Sect. 8.9) was used to calculate the integral of dF/dE , and the results were fitted to the experimental data given in Table 10.2.1. The value of B for the best fit is $0.0140 \pm 0.0005 \text{ g cm}^{-2} \text{ Mev}^{-1}$.

From the data of Flynn⁸ an experimentally governed relationship dT/dE , where T is the total light output in electron-produced equivalent light, has been calculated. A fit to his data required consideration of both fast and slow components of the light output, as follows:

$$\frac{dT}{dE} = (1 - R) \frac{dF}{dE} + R \frac{dS}{dE}, \quad (2)$$

where R is the fraction of total light which exists in the slow component. Various relationships have been tested for dS/dE as a function of dE/dX . A Birks-like relation, similar to Eq. (1), did not give a good fit. Better results were obtained by using

$$\frac{dS}{dE} = \exp\left(-B' \frac{dE}{dX}\right). \quad (3)$$

When the data of Flynn were fitted to Eq. (2), using Eq. (3) to obtain dS/dE , a value of $R = 0.34 \pm 0.04$ and a value of $B = 0.0012 \pm 0.0001 \text{ g cm}^{-2} \text{ Mev}^{-1}$ were obtained, but it appeared that too much "slow" light existed systematically at the lower energies.

Attempts to find a better fit for $T(E)$ led to the following modification of Eq. (3):

$$\frac{dS}{dE} = \begin{cases} \exp\left(-B' \frac{dE}{dX}\right); & E > E_{\text{cut}} \\ 0; & E \leq E_{\text{cut}} \end{cases}, \quad (4)$$

where E_{cut} is an empirically introduced cutoff energy equal to one-half the energy at which dE/dX is maximum, or about $\frac{1}{4}$ Mev for alpha particles. This represents an approximation to the fact that light production is not related to the true dE/dX as measured by the energy loss, but to the electronic stopping power (ϵ_{elec}), which can be much less than the nuclear stopping power (ϵ_{nuc}) at very low energy. This empirical formulation is in best agreement with the data of this experiment at $R = 0.3$ and $B' = 0.0014 \text{ g cm}^{-2} \text{ Mev}^{-1}$ and yields a better fit than can be obtained by using Eq. (3).

References

¹Centre D'Etudes Nucleaires, Fontenay-aux-Roses, France.

²M. Forte *et al.*, p. 277 in *Proceedings of Conference on Nuclear Electronics, Vienna, Vol. 2*, International Atomic Energy Agency, Vienna, 1962.

³F. D. Brooks, *Nucl. Instr. Methods* **4**, 151 (1959).

⁴R. B. Owen, *IRE Trans. Nucl. Sci.* **NS-5**, 198 (1958).

⁵R. W. Peelle and T. A. Love, p. 196 in *Conference on Instrumentation Techniques in Nuclear Pulse Analysis, 2nd, Monterey, 1963*, Nuclear Science Series No. 40, National Academy of Science, Washington, D.C., 1964.

⁶Nuclear Enterprises, Ltd., Winnipeg, Canada.

⁷J. B. Birks *et al.*, *Proc. Phys. Soc. (London)* **A64**, 879 (1951).

⁸K. F. Flynn *et al.*, *Nucl. Instr. Methods* **27**, 13 (1964).

10.3. MODIFICATION OF A 400-CHANNEL PULSE-HEIGHT ANALYZER TO ELIMINATE STORAGE OF PULSES HAVING ENERGIES BELOW A PRESET BIAS

H. A. Todd¹

T. A. Love

An undesirable phenomenon has been encountered in using a commercial transistorized 400-channel pulse-height analyzer² to measure pulse-height spectra above an arbitrarily preset energy level: even though the pulses correspond to energies below the preset level, they are, nevertheless,

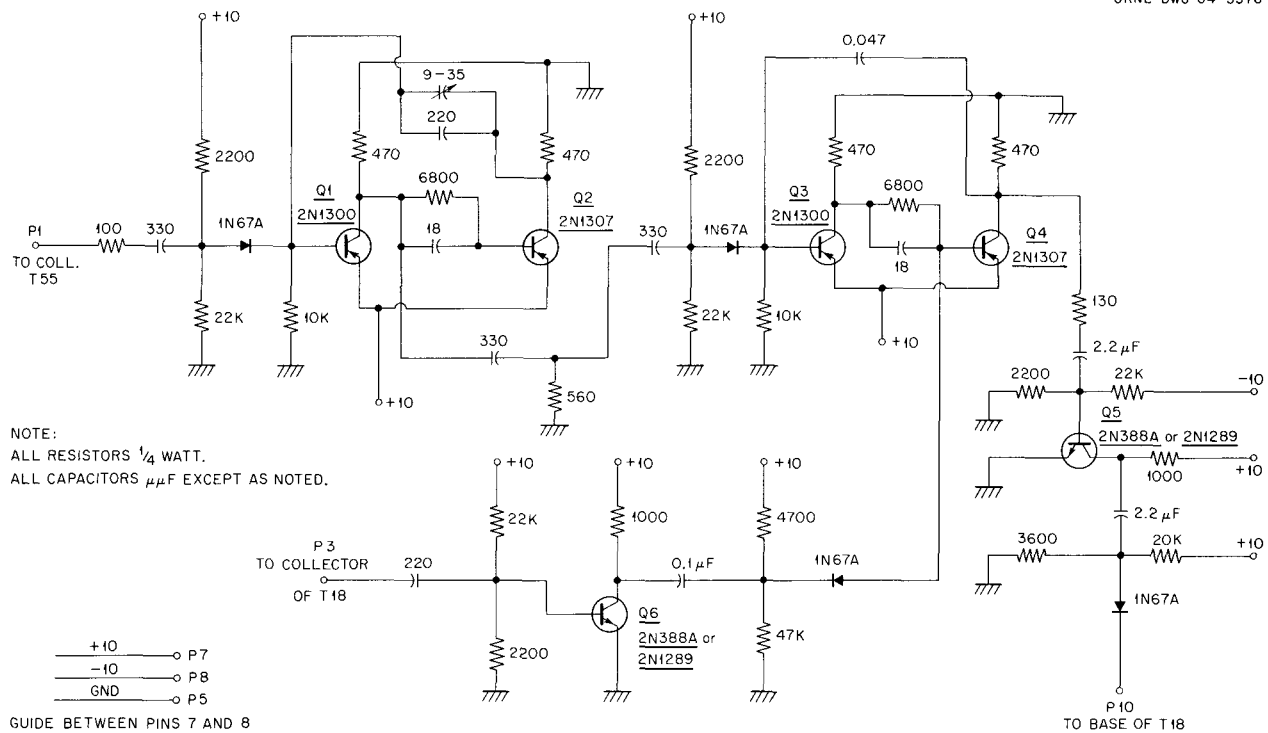


Fig. 10.3.1. Circuit for Elimination of Storage of Pulses Below a Preset Trigger Level in a 400-Channel Analyzer.

stored, the rate at which they are stored being proportional to the number of such pulses present in the spectrum. This erroneous storage occurs when the analyzer is triggered externally, as well as when it is triggered internally with the sensitivity, set to reject small pulses, and it is apparently caused by the trigger opening the linear gate $\sim 2 \mu\text{sec}$ before the concurrent signal reaches the gate. Any pulse arriving at the linear gate during this $2\text{-}\mu\text{sec}$ period is stretched, and a signal is applied to the collector of the Shaper 1 circuit (familiarity with analyzer terminology is assumed), which results in the linear gate being closed before the desired signal has reached it.

The circuit shown in Fig. 10.3.1 has been designed to overcome this difficulty. The circuit clamps the base of Shaper 1 (designated as T18) for $\sim 2 \mu\text{sec}$, thereby preventing the linear gate from being closed until after the desired signal reaches it. The trigger pair Q1 and Q2 has a

natural period of from 1.8 to $2.1 \mu\text{sec}$, while the trigger pair Q3 and Q4 has a natural period longer than any pulse storage time possible in the analyzer. A pulse from the trailing edge of the Shaper 1 collector waveform is used to reset trigger pair Q3 and Q4 to its quiescent state at the end of conversion.

The successful performance of the circuit is demonstrated by the two measurements of the pulse-height spectrum of ^{60}Co gamma rays shown in Fig. 10.3.2. Both measurements reflect a count rate of $\sim 12,000$ counts/sec, corresponding to an analyzer dead time of $\sim 50\%$. It is clear that the installation of the clamping circuit has completely eliminated the accumulation of undesired pulses in the lower numbered channels.

The modified analyzer has been tested at count rates varying from 300 to 12,000 counts/sec and with trigger delays varying over a range of $\pm 0.5 \mu\text{sec}$. Its performance was uniformly satisfactory.

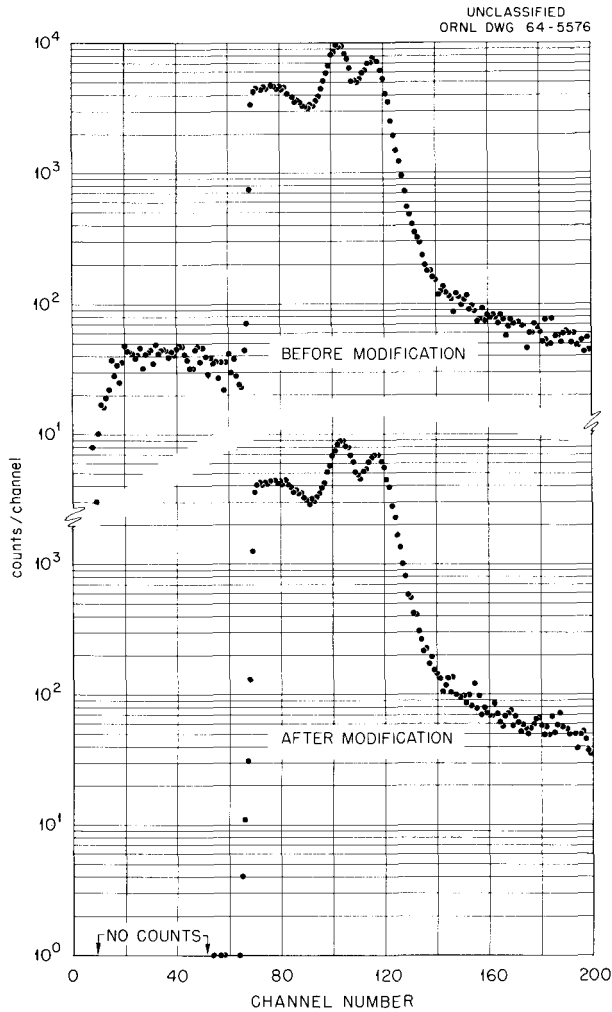


Fig. 10.3.2. Pulse-Height Spectra of ^{60}Co Gamma Rays Before and After Modification of the 400-Channel Analyzer.

References

- ¹Instrumentation and Controls Division.
²Radiation Instrument Development Laboratory Model 34-12.

10.4. THE CHOICE OF CAPACITORS FOR NANOSECOND CIRCUITS¹

N. W. Hill² C. O. McNew²

A precision pulse generator has been used in conjunction with a sampling oscilloscope and

suitable jigs to measure the stray capacitance and inductance of a variety of capacitors suitable for bypassing and coupling applications in nanosecond circuitry. For these tests all lead lengths were held to less than $\frac{1}{16}$ in., so that the inductances measured were due to leads and plates within the capacitors themselves. Three types of capacitors were tested: ceramic, silvered mica, and tantalum electrolytic. Little difference was found in the inductances of all three types as long as the lead lengths were held to essentially zero. The minimum values were obtained for feed-through and coaxial types, which, however, are special types and require specialized mounting techniques when employed. It was found that essentially the same results could be achieved if more standard types were used in parallel.

A literature survey was made to accumulate basic data relative to characteristics of various types of capacitors under various conditions of voltage, frequency, temperature, and humidity.

References

- ¹Abstract of ORNL-TM-999 (in press).
²Instrumentation and Controls Division.

10.5. PROGRESS IN THE DEVELOPMENT OF AN INSTRUMENT-RESPONSE UNFOLDING METHOD

W. R. Burrus B. D. Holcomb¹
 J. Replogle¹

Over the past several years an instrument response unfolding method has been developed. The essential idea is to predict, or estimate, from measured analyzer data what the response of an ideal analyzer would be. Of course, the ideal analyzer must not be assumed to have too good a resolution, since the use of data obtained on a real analyzer with moderate resolution would result in estimates with a broad confidence interval. In neutron or gamma-ray spectroscopy, one would like to have an instrument with a single narrow Gaussian-type response function with no spurious peaks or tails – thus the ideal analyzer is taken to have a resolution about equal to the inherent resolution of the actual analyzer. In more subtle

analyses, such as the determination of neutron spectra from threshold foils, it is assumed that a set of threshold foils with abrupt thresholds is desired. Then the aim would be to predict or estimate from actual data what the ideal foils would indicate.

The method consists in constructing the intersection of two mathematical regions: (1) the joint confidence region for the response of the hypothetical analyzer, which is obtained from ordinary linear estimation theory, and (2) the confidence region due to *a priori* constraints upon the spectrum (such as nonnegativity or some intrinsic broadening process). The final confidence region is then the one where these two regions overlap. This constrained estimation problem can be posed as a problem in parametric-quadratic programming and can be approximated by a linear programming problem or a modified least-squares problem (SLOP program).² The solution to the quadratic problem yields the optimum result, that is, the smallest confidence interval, and the estimation efficiency of the other approximations is judged by comparing the confidence intervals they produce with the optimum.

The treatment outlined above has been applied to experimental data obtained with a variety of neutron and gamma-ray spectrometers. Among them have been a total-absorption gamma-ray spectrometer using an NaI(Tl) crystal,³ proton-recoil neutron spectrometers using liquid (NE-213) and plastic (Pilot B) scintillators,⁴ a Bonner-sphere neutron spectrometer,³ total-absorption anti-coincidence and multicrystal pair gamma-ray spectrometers (Sect. 9.3), a recoil proton telescope, and a dE/dx high-energy proton spectrometer.

Current problems include the determination of neutron spectra from threshold foil data, the analysis of radioactive decay, where the decay curve is a sum of exponentials, and the analysis of data obtained by lithium-drifted-diode solid-state spectrometers. Although the last three problems are not so susceptible to straightforward analysis as the earlier ones are, we believe that the method described has a potentially greater advantage over older methods.

The data for all the above problems are prepared in essentially the same form. The input consists of a description of the response function of the actual experimental instrument, a description of the *a priori* constraints upon the spectrum, a description of the ideal analyzer for which results are to

be estimated, and the count distribution resulting from the experiment.

Although the preparation of the input data (pre-unfolding) is quite different for the various problems, the same unfolding code can in principle be used for all. Although some attention must be paid to the unfolding portion of the code in order to optimize the computer time vs estimation efficiency of the results, preparation of the input data has proved to be the most time-consuming and difficult stage.

In addition to the solution of practical problems, we have constructed experimental versions of the following new algorithms which have been tested in small but fairly difficult test cases.

1. A quadratic programming code which, although not fast enough for routine application, is expected to serve as a standard of comparison for other approximate methods.

2. Several variants of the linear programming approximation, with the aim being to reduce the amount of computation from the order of n^4 (n is the typical dimension of the problem in matrix form) to n^3 . Although not yet completely satisfactory, the best of the new algorithms is an order of magnitude faster than last year's linear programming algorithm.

3. A new version of the SLOP code which combines selected features of the least-squares method and the programming method. The experimental version of this code is complete but not yet entirely satisfactory.

We now plan to give greatest emphasis to the completion of a "publication version" of a simplified modified least-squares code which will be well documented and easy to use. This will be followed by an improved and expanded SLOP code and a linear programming code. We have found that the task of writing a FORTRAN code that is compatible with both FORTRAN-63 and FORTRAN-4, an earlier goal, is virtually impossible; however, the simple code will be nearly compatible.

References

¹Central Data Processing Facility of the Oak Ridge Gaseous Diffusion Plant.

²V. D. Bogert and W. R. Burrus, *Neutron Phys. Div. Ann. Progr. Rept. Sept. 1, 1962*, ORNL-3360, p. 22.

³W. R. Burrus, *Neutron Phys. Div. Ann. Progr. Rept. Sept. 1, 1962*, ORNL-3360, p. 19.

⁴W. R. Burrus, *Neutron Phys. Div. Ann. Progr. Rept. Aug. 1, 1963*, ORNL-3499, Vol. II, p. 120.

10.6. A SENSITIVE TUNNEL-DIODE DISCRIMINATOR¹

N. W. Hill²

Recently available ultrahigh-speed germanium tunnel diodes with very low junction capacitance make it possible to design highly sensitive discriminators or threshold circuits for use with pulses having rise and fall times of a few nanoseconds. A tunnel-diode discriminator module is described which permits the detection of 2-mv 3-nsec rise time photomultiplier pulses. The precautions required with regard to input-output terminations, both within the discriminator circuit and in the circuits which follow it, and with regard to regulation of power supplies against line and load variations are listed.

References

¹Abstract of ORNL-TM-998 (in press).

²Instrumentation and Controls Division.

10.7. STRIP-LINE CONSTRUCTION FOR NANOSECOND CIRCUITRY

J. W. McConnell¹

The trend toward the use of faster electronic circuits in nuclear experiments has dictated the use of microwave techniques in circuit layout. In order to minimize the effects of stray capacitance and lead inductance, it is desirable to build active circuits into a transmission line system. Two types of strip lines have been studied, and experimental data have been obtained concerning the characteristic impedance of a commercial copper-clad dielectric.²

Microstrip construction, shown diagrammatically in Fig. 10.7.1a, lends itself most readily to the insertion of lumped components. This type of construction, however, has two major disadvantages: adequate theoretical relationships between characteristic impedance and geometrical dimensions are lacking, and shielding from external fields is relatively poor. Some theoretical considerations for this type of construction have been developed by Assadourian and Rimai³; however, only two cases appear to be amenable to analysis, and, unfortunately, the approximation in both cases is not very good in the impedance range (50–125 ohms) of interest. Figures 10.7.2 and 10.7.3 show comparisons between calculated and measured impedances as functions of conductor width for nominal dielectric thicknesses of $\frac{1}{16}$ and $\frac{1}{8}$ in. respectively. In all cases the width of the ground plane was approximately four times the width of the conductor. Pulse reflection techniques were used to measure impedance, with a 50-ohm General Radio air line as a comparison standard.

UNCLASSIFIED
2-01-058-940

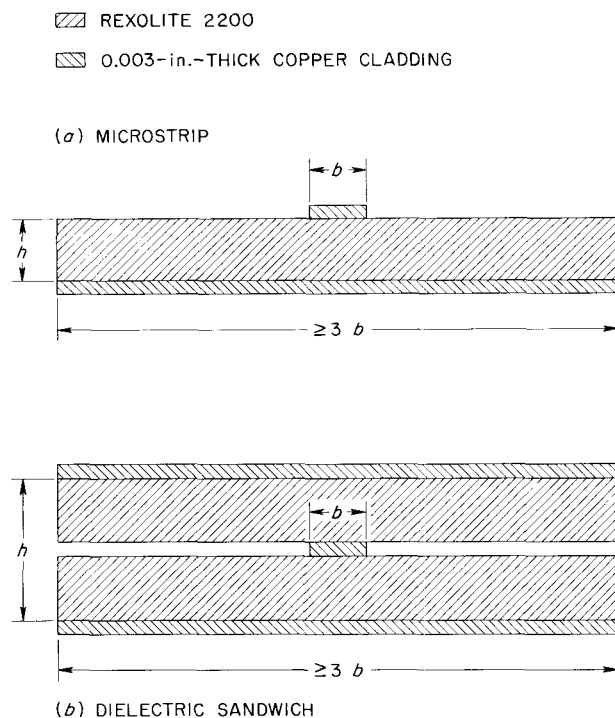


Fig. 10.7.1. Strip-Line Cross Sections: (a) Microstrip; (b) dielectric sandwich.

Table 10.7.1. Comparison of Measured and Calculated Impedances of a Dielectric-Sandwich Transmission Line

Sandwich Thickness, ^a <i>h</i> (in.)	Conductor Width, ^a <i>b</i> (in.)	Impedance (ohms)	
		Measured	Calculated
0.119	0.077	53.1	50
0.245	0.164	53.5	50
0.245	0.036	103	100

^aSee Fig. 10.7.1.

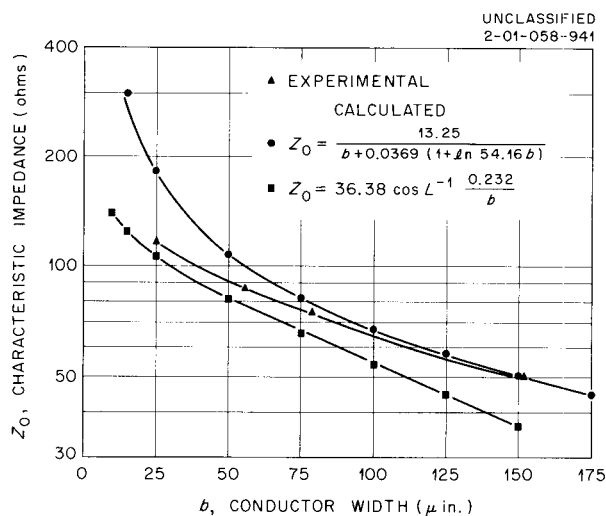


Fig. 10.7.2. Characteristic Impedance as a Function of Conductor Width for 1/16-in.-thick Rexolite-2200.

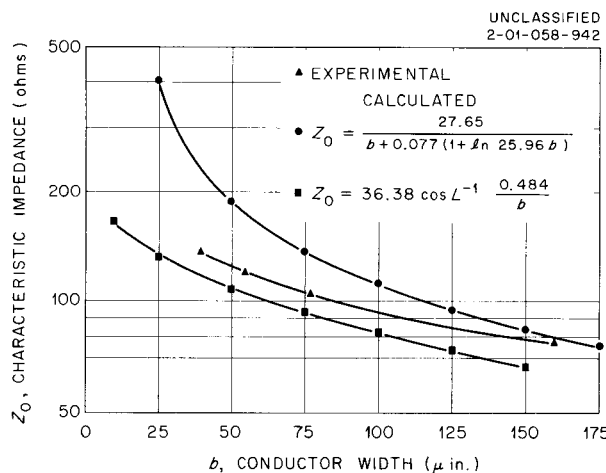


Fig. 10.7.3. Characteristic Impedance as a Function of Conductor Width for 1/8-in.-thick Rexolite-2200.

Dielectric-sandwich construction, shown in Fig. 10.7.1b, has the advantage of excellent shielding from external fields. Its obvious disadvantage, of course, is the difficulty in inserting lumped components into the system. This type of construction can be analyzed mathematically, however, and a relatively simple technique which utilizes the fringe capacitance approach has been given by Cohn.⁴ Impedances calculated by this method are compared in Table 10.7.1 with measured impedances for three typical dielectric-sandwich lines. The agreement between experiment and calculation is good.

References

- ¹Instrumentation and Controls Division.
- ²Rexolite 2200: a thermosetting, styrene-base copolymer manufactured by the Brand Rex Division of American Enka Corp.
- ³F. Assadourian and E. Rimai, *IRE Proc.* **40**, 1651 (1952).
- ⁴S. B. Cohn, *IRE Trans. MTT-2*(2), 52 (1954).

10.8. PERFORMANCE CHARACTERISTICS OF MODULAR NANOSECOND CIRCUITRY EMPLOYING TUNNEL DIODES¹

N. W. Hill²

J. W. McConnell²

R. J. Scroggs³

J. M. Madison²

Tunnel diodes have been used in the design and construction of a variety of modular circuitry used in instrumentation for high-energy particle experiments. Modules included fast- and slow-recovery

discriminators, fast- and slow-recovery coincidence modules, positive- and negative-output scaler drivers, and a 100-Mc scaler driver. The individual univibrators used in the circuitry and the completed modules have been subjected to extensive tests to determine the effects of variations in operating temperature and in input pulse magnitude on resolution, pulse shape, walk, and thresholds.

It was found that circuitry using tunnel diodes is strongly affected by such variations, as well as by fluctuations in the power supply. It was also noted that parameter differences between supposedly identical tunnel diodes produced significantly large variations in module behavior.

It is concluded that the modular circuits discussed and shown in this report are satisfactory for their intended purposes, but that maximum performance and stability can be assured only by individual selection and testing of the tunnel diodes and by regulation of power supplies to $\pm 0.01\%$ for both line and load.

References

¹Abstract of ORNL-3687 (October 1964).

²Instrumentation and Controls Division.

³Now at Oak Ridge Technical Enterprises Corp., Oak Ridge, Tenn.

10.9. CURLED LIGHT PIPES FOR THIN ORGANIC SCINTILLATORS¹

W. A. Gibson

An economical technique has been devised for fabricating efficient light pipes to transmit light from a thin, disk-like organic scintillator to the cathode of a photomultiplier. In this technique the starting material consists of a thin rectangle of Lucite having a width and thickness slightly greater than the diameter and thickness of the scintillator respectively. One end of the rectangle is cut to fit the edge of the scintillator, and the cut edge is highly polished. The other end of the Lucite is softened, by immersion in heated mineral oil, and then immediately curled around a cylinder of suitable diameter. The radius of the cylinder is chosen to be well within the radius of the photocathode with which the light pipe is to be

used. Sanding and polishing of the curled end of the light pipe complete its fabrication. Comparisons of the transmission of curled light pipes and of a solid-block Lucite pipe showed the curled pipe to be somewhat better, both in transmission efficiency and in resolution.

References

¹Abstract of published paper: *Rev. Sci. Instr.* **35**, 1021 (1964).

10.10. NANOSECOND LIGHT SOURCES FOR GAIN STABILIZATION¹

J. W. McConnell²

It is well known that the gain of photomultiplier tubes changes with time, temperature, count rate, and magnetic field. Amplifiers and pulse-height analyzers may also exhibit drifts, particularly during long runs. However, the gain of a complete system employing a photomultiplier tube can be stabilized by injecting a stable light pulse into the photomultiplier and using this signal as a reference in a feedback loop. Three fast light sources — a corona lamp, an argon lamp, and a high-pressure neon lamp — were tested as possible sources for such a pulse.

The commercial corona lamps tested gave a nearly ideally shaped light pulse but were too unstable in light output for use as a standard source. The argon lamp system showed good stability, but the light pulse possesses a long, low-amplitude tail which introduces difficulties in high-gain systems. The most promising source appears to be the high-pressure (190-mm Hg) neon lamp for which preliminary tests show a suitable pulse shape, output, and duration. While no accurate measurement of the stability of the neon lamp has been made, it is obviously much better than that of the corona lamp.

Since fast-rising, high-voltage pulses are required to excite all three light sources, it is important that all components be thoroughly and well shielded.

References

¹Abstract of ORNL-TM-985 (in press).

²Instrumentation and Controls Division.

10.11. A METHOD FOR MAKING INEXPENSIVE THICK BORON TARGETS TO OBTAIN GAMMA RAYS FROM THE $^{11}\text{B}(p,\gamma)^{12}\text{C}$ REACTION¹

R. T. Santoro H. Weaver

An inexpensive method has been devised for the preparation of ^{11}B accelerator targets used for the production of 4.43- and 11.7-Mev gamma rays from the $^{11}\text{B}(p,\gamma)^{12}\text{C}$ reaction. A 1-in.-diam target prepared by the method gave the same number of counts in the 4.43- and 11.7-Mev gamma-ray peaks as were given by a ^{11}B target prepared by the usual evaporation method. In addition, the inexpensive target was unchanged after an 8-hr run, while the evaporated target showed damage by flaking after being in an accelerator beam for 2 to 4 hr.

References

¹Abstract of a "Letter to the Editor" accepted for publication in *The Review of Scientific Instruments*.

10.12. CONSTANT-CURRENT SOURCES FOR INSTRUMENT CALIBRATION

R. T. Santoro R. J. Scroggs²
F. E. Gillespie¹ T. A. Love

A constant-current source for use in calibrating electrometers and current-integrating instruments has been designed, and two sources have been built. The need for such a calibration source arose during proton beam intensity measurements made at the Harvard University Synchrocyclotron (Sect. 9.2), and the sources will be used as calibration standards in future measurements of the same type (Sect. 9.8).

The current source consists of a parallel plate ionization chamber with one electrode coated with an alpha emitter, ^{241}Am . The alpha source is doubly contained, and the ionization chamber is shock-mounted. The device is filled with argon at an absolute pressure of 80 cm Hg. Saturation is achieved at low voltage, as shown by the typical saturation curve of Fig. 10.12.1. The current output due to background radiation is reduced by minimum spacing of the electrodes and by lining the source with lead.

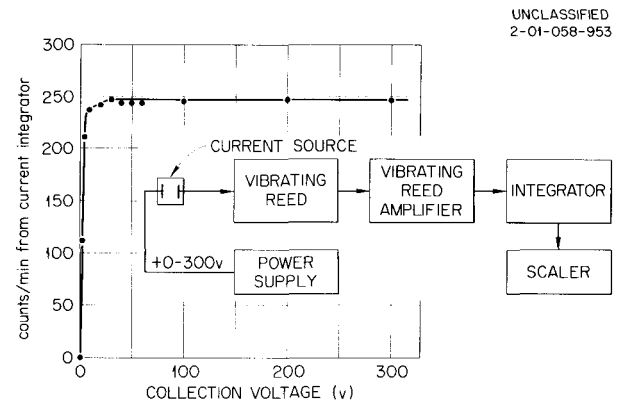


Fig. 10.12.1. Typical Saturation Curve for Constant-Current Sources. The diagram shows the experimental arrangement used to obtain the data.

The current output of the weaker source has been measured as 3×10^{-12} amp, with approximately 800 dis/sec; and that of the stronger source as 7×10^{-11} amp, with 1.3×10^4 dis/sec, both at an applied voltage of 150 v. Tested over a period of six months, the current drift was less than 1%. The precise values of current and drift have been measured.

Reference

¹Instrumentation and Controls Division.
²Oak Ridge Technical Enterprises Corp., Oak Ridge, Tenn.

10.13. CALCULATION OF THE EFFICIENCY OF ORGANIC SCINTILLATORS FOR FAST NEUTRONS

R. J. Schuttler¹

Except for a recent paper by R. J. Kurz,² calculations which have been reported for the neutron detection efficiency of organic scintillators have been largely concerned with the neutron energy region below 15 Mev. The calculation reported here was initiated in support of flight-time neutron spectrometric measurements³ in the region up to 50 Mev, or perhaps even higher.

The problem of estimating counting efficiencies is made complex by the finite counting threshold for the pulses that arise from the various neutron interactions in the scintillator; each interaction leads to charged particles for which there is a different relationship between deposited energy and the resulting pulse height. For some scintillators, including the type used in the flight-time neutron spectroscopy experiments, the time dependence of the resulting pulse depends upon the characteristics of the exciting radiation, so that the behavior of both fast and slow components of the light must be understood. In a typical reaction of a neutron with carbon, two or more charged particles may give up energy in the phosphor, and the resulting pulse height will depend upon the division of energy between these products.

This complicated situation, together with inadequate cross-section information for the important reactions, has led to the use of data from theoretical calculations⁴ based on a simple nuclear model and free-particle empirical cross sections. This approach is valuable for the region above about 12 Mev, where the reactions in the carbon of the scintillator are likely to be important; below this energy one may use techniques which depend on interactions with hydrogen only. The size of the scintillator enters into the computation only in the consideration of the interaction of any secondary neutrons; thus the attenuation of the primary neutron beam is handled separately from the main process. Problems connected with edge effect and pulses from carbon recoils have been assessed.

The computation is based on a modified combination of history magnetic tapes from the intranuclear cascade program of Bertini⁴ (neutrons on ^{12}C) with the evaporation program of Dresner⁵ and with formulas giving the light output predicted for the absorption of energy from the various charged particles emitted. At the low incident energies of interest to this work, the differences in nucleon separation energy from one element to the next are important, and it was necessary to interpret the intranuclear cascade history tapes in an un-

orthodox manner to reduce the importance of energetically impossible reactions. It happens that the Bertini program records the cascade particles leaving the nucleus more or less in order of decreasing energy; so in analyzing the history tapes the present program is able to compute the apparent excitation energy of the tentative residual nucleus after taking into account each successive escaping nucleon. Escaping particles are not included if they force a negative excitation energy. While this modification makes little difference to the number of escaping cascade particles from a medium-weight nucleus bombarded at high energies, it makes an important difference for carbon bombarded with neutrons in the 15- to 50-Mev range. A study of the predicted pulse-height spectra and the corresponding radiochemical yields shows that this method gives a reasonable account of most of the reactions of importance in the scintillator, although it does not give enough prominence to the $^{12}\text{C}(n,\alpha)^9\text{Be}$ reaction which is important at 14 Mev as judged from the pulse-height spectra observed in a scintillator. The efficiency estimates resulting from this work are being assessed.

References

¹Centre D'Etudes Nucleaires, Fontenay-aux-Roses, France.

²R. J. Kurz, *A 709/7090 Fortran-II Program to Compute the Neutron-Detection Efficiency of Plastic Scintillators for Neutron Energies from 1 to 300 MeV*, UCRL-11339 (1964).

³R. W. Peelle *et al.*, *Neutron Phys. Div. Ann. Progr. Rept. Aug. 1, 1963*, ORNL-3499, Vol. II, p. 66.

⁴H. Bertini, *Phys. Rev.* **131**, 1801 (1963).

⁵L. Dresner, *EVAP - A FORTRAN Program for Calculating the Evaporation of Various Particles from Excited Compound Nuclei*, ORNL-CF-61-12-30 (December 1961).

INTERNAL DISTRIBUTION

1. L. S. Abbott
2. F. S. Alsmiller
3. R. G. Alsmiller, Jr.
4. J. Barish (K-25)
5. H. W. Bertini
6. N. A. Betz
- 7-46. E. P. Blizard
47. T. V. Blosser
48. M. S. Bokhari
49. W. R. Burrus
50. V. R. Cain
51. A. D. Callihan
52. G. T. Chapman
53. H. C. Claiborne
54. F. H. Clark
55. C. E. Clifford
56. W. Coleman
57. J. C. Courtney
58. R. R. Coveyou
59. G. deSaussure
60. J. K. Dickens
61. L. Dresner
62. M. B. Emmett
63. K. Franz (K-25)
64. R. M. Freestone, Jr.
65. J. Gibbons
66. W. A. Gibson
67. F. E. Gillespie
68. J. H. Gillette
69. M. Guthrie
70. R. Gwin
71. V. M. Hamrick
72. J. A. Harvey
73. R. M. Haybron
74. K. M. Henry, Jr.
75. N. W. Hill
76. B. D. Holcomb (K-25)
77. L. B. Holland
78. J. L. Hull
79. D. Irving
80. E. B. Johnson
81. W. H. Jordan
82. L. Jung
83. F. B. K. Kam
84. M. M. Kedle
85. W. E. Kinney
86. K. A. Kraus
87. C. E. Larson
88. M. Leimdorfer
89. J. Lewin
90. T. A. Love
91. R. L. Macklin
92. J. M. Madison
93. R. E. Maerker
94. D. W. Magnuson
95. F. C. Maienschein
96. J. J. Manning
97. B. F. Maskewitz
98. J. W. McConnell
99. B. McGill
100. C. O. McNew
101. S. K. Mehta
102. J. T. Mihalcz
103. J. M. Miller
104. H. S. Moran
105. F. J. Muckenthaler
- 106-107. R. B. Parker
108. R. W. Peelle
109. S. K. Penny
110. C. M. Perey
111. F. J. Perey
112. S. J. Rafferty
113. R. J. Raridon
114. J. Repolgle (K-25)
115. B. Rust (K-25)
116. G. R. Satchler
117. R. T. Santoro
118. R. J. Scroggs
119. R. J. Silva
120. E. G. Silver
121. M. J. Skinner
122. G. G. Slaughter
123. R. D. Smiddie
124. W. R. Smith
125. J. G. Sullivan
126. J. A. Swartout
127. T. Tamura
128. J. T. Thomas
129. H. A. Todd
130. D. K. Trubey
131. V. V. Verbinski
132. J. Wachter

- | | |
|---------------------------------|---|
| 133. D. R. Ward | 143. G. Dessauer (consultant) |
| 134. J. W. Webster | 144. M. L. Goldberger (consultant) |
| 135. A. M. Weinberg | 145. Radiation Shielding Information Center |
| 136. L. W. Weston | 146. Biology Library |
| 137. E. P. Wigner | 147-149. Central Research Library |
| 138. G. C. Williams | 150. Reactor Division Library |
| 139. Gale Young | 151-152. ORNL-Y-12 Technical Library,
Document Reference Section |
| 140. W. Zobel | 153-487. Laboratory Records Department |
| 141. R. A. Charpie (consultant) | 488. Laboratory Records, ORNL R.C. |
| 142. R. F. Taschek (consultant) | |

EXTERNAL DISTRIBUTION

489. Research and Development Division, AEC, ORO
490-1135. Given distribution as shown in TID-4500 (35th ed.) under Physics Category (75 copies – CFSTI)